Experimental and modeling studies on the Ru/C catalyzed levulinic acid hydrogenation to γ–valerolactone in packed bed microreactors

Hommes, Arne; Horst, ter, Arjan; Koeslag, Meine; Heeres, Hero; Yue, Jun

Published in:
Chemical Engineering Journal

DOI:
10.1016/j.cej.2020.125750

Publication date:
2020

Chemical Engineering Journal 399 (2020) 125750

Contents lists available at ScienceDirect

Chemical Engineering Journal

journal homepage: www.elsevier.com/locate/cej

Experimental and modeling studies on the Ru/C catalyzed levulinic acid hydrogenation to γ-valerolactone in packed bed microreactors

Arne Hommes, Arie Johannes ter Horst, Meine Koeslag, Hero Jan Heeres, Jun Yue*

Department of Chemical Engineering, Engineering and Technology Institute Groningen, University of Groningen, Nijenborgh 4, 9747 AG Groningen, the Netherlands

HIGHLIGHTS

- Hydrogenation of levulinic acid over Ru/C was tested in microreactors.
- 100% levulinic acid conversion and 84% γ-valerolactone yield were obtained.
- A microreactor model was developed to describe mass transfer and kinetics.
- Reaction rate was limited by external liquid–solid mass transfer of H_2.
- A microreactor optimization strategy was proposed.

GRAPHICAL ABSTRACT

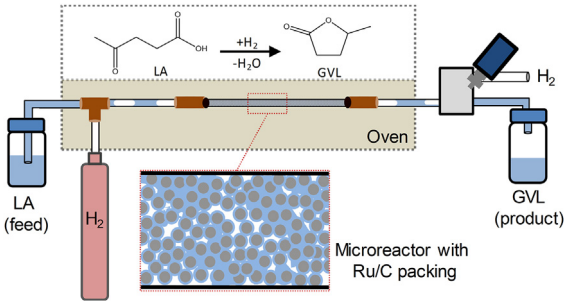

ARTICLE INFO

Keywords:
Gas-liquid-solid
Hydrogenation
Levulinic acid
Mass transfer
Packed bed microreactor
γ-Valerolactone

ABSTRACT

The hydrogenation of levulinic acid (LA) to γ-valerolactone (GVL) was performed in perfluoroalkoxy alkane capillary microreactors packed with a carbon-supported ruthenium (Ru/C) catalyst with an average particle diameter of 0.3 or 0.45 mm. The reaction was executed under an upstream gas–liquid slug flow with 1,4-dioxane as the solvent and H_2 as the hydrogen donor in the gas phase. Operating conditions (i.e., flow rate and gas to liquid flow ratio, pressure, temperature and catalyst particle size) were varied in the microreactor to determine the influence of mass transfer and kinetic characteristics on the reaction performance. At 130 °C, 12 bar H_2 and a weight hourly space velocity of the liquid feed (*WHSV*) of 3.0 $g_{feed}/(g_{cat}{\cdot}h)$, 100% LA conversion and 84% GVL yield were obtained. Under the conditions tested (70–130 °C and 9–15 bar) the reaction rate was affected by mass transfer, given the notable effect of the mixture flow rate and catalyst particle size on the LA conversion and GVL yield at a certain *WHSV*. A microreactor model was developed by considering gas–liquid–solid mass transfer therein and the reaction kinetics estimated from the literature correlations and data. This model well describes the measured LA conversion for varying operating conditions, provided that the internal diffusion and kinetic rates were not considered rate limiting. Liquid–solid mass transfer of hydrogen towards the external catalyst surface was thus found dominant in most experiments. The developed model can aid in the further optimization of the Ru/C catalyzed levulinic acid hydrogenation in packed bed microreactors.

1. Introduction

Biomass is an abundantly available and renewable source of carbon with potential to replace fossil (petroleum) sources in the production of chemicals and fuels [1]. One of the most promising biobased platform chemicals is levulinic acid (LA) [2,3], which is typically produced by the acid-catalyzed rehydration of furans (i.e., 5-hydroxymethylfurfural (HMF) or furfuryl alcohol) derived from C_5- and C_6-sugars obtained

* Corresponding author.
E-mail address: yue.jun@rug.nl (J. Yue).

https://doi.org/10.1016/j.cej.2020.125750
Received 10 April 2020; Received in revised form 20 May 2020; Accepted 1 June 2020
Available online 06 June 2020

Nomenclature

a_c	Specific catalyst surface area (m^2/g_{cat})
a_i	Specific gas–liquid interfacial area (m^2/m^3)
A	Pre-exponential factor for (0.5, 0)-order ($((mol{\cdot}L)^{0.5}/(g_{cat}{\cdot}s)$) or for (0.5, 1)-order reaction ($((L^3/mol)^{0.5}/(g_{cat}{\cdot}s)$)
A_c	Surface area of catalyst particles (m^2)
C	Concentration (mol/m^3)
d	Diameter (m)
D	Mass diffusivity (m^2/s)
D_{eff}	Effective diffusivity (m^2/s)
E_a	Activation energy (J/mol)
H	Henry coefficient (–)
j	Superficial velocity ($= 4Q/\pi d_C^2$) (m/s)
k	Overall reaction rate constant for (0.5, 0)-order ($((mol{\cdot}L)^{0.5}/(g_{cat}{\cdot}s)$) or for (0.5, 1)-order reaction ($((L^3/mol)^{0.5}/(g_{cat}{\cdot}s)$)
k_L	Liquid phase mass transfer coefficient (m/s)
k_S	Liquid–solid mass transfer coefficient (m/s)
L	Length (m)
m	mass flow rate (kg/s)
p	Pressure (Pa)
Q	Volumetric flow rate (m^3/s)
r	Rate of transfer (mol/s)
r'	Rate of transfer per unit mass of catalyst ($mol/(g_{cat}{\cdot}s)$)
T	Temperature (°C or K)
V	Volume (m^3)
w_c	Catalyst weight (g)
$WHSV$	Weight hourly space velocity ($g_{feed}/(g_{cat}{\cdot}h)$ or $g_{LA}/(g_{cat}{\cdot}h)$)
X	Conversion (%)
Y	Yield (%)

Greek letters

α	Wetted catalyst fraction (–)
γ	Surface tension (N/m)
ε	Bed porosity (–)
η	Effectiveness factor (–)
μ	Dynamic viscosity (Pa·s)
ρ	Density (g/m^3)
σ	Selectivity (%)
ϕ	Thiele modulus (–)
χ_G	Lockhart-Martinelli ratio ($= j_G\sqrt{\rho_G}/(j_L\sqrt{\rho_L})$) (–)

Subscripts

0	At the packed bed microreactor inlet
1	At the packed bed microreactor outlet
B	In the bulk
c	Catalyst
C	Capillary microreactor
G	Gas
GVL	γ-Valerolactone
HPA	4-Hydroxypentanoic acid
I	At the interface
L	Liquid
LA	Levulinic acid
p	Particle
S	Surface reaction

Dimensionless numbers

Re	Reynolds number ($= \rho j d_p/\mu$)
Sc	Schmidt number ($= \mu/(\rho D)$)
Sh	Sherwood number ($= k_S d_p/D$)
We	Weber number ($= \rho j^2 d_p/\gamma$)

Abbreviations

α-AL	α-Angelicalactone
CTFE	Chlorotrifluoroethylene
GVL	γ-Valerolactone
HPA	4-Hydroxypentanoic acid
LA	Levulinic acid
LIC	Liquid level indicator/controller
MFC	Mass flow controller
MTHF	2-Methyltetrahydrofuran
PEEK	Polyether ether ketone
PFA	Perfluoroalkoxy alkane
PTFE	Polytetrafluoroethylene
Ru/C	Carbon-supported ruthenium
WHSV	Weight hourly space velocity

from (hemi-)cellulosic biomass [4]. LA can be converted into a large variety of chemicals. Its catalytic hydrogenation/dehydration results in γ-valerolactone (GVL), with potential uses as food or fuel additive [5–7]. GVL is also a non-toxic solvent [5,8], with reported applications in e.g., the homogeneous acid catalyzed production of LA from cellulose [9], the heterogeneously catalyzed synthesis of HMF from glucose [10] and microwave-assisted peptide synthesis [11]. Furthermore, GVL can be converted into a variety of value-added products including solvents (e.g., alkyl 4-alkoxyvalerates) [12], polymer precursors (e.g., dimethyl adipate for producing nylons and α-methylene-γ-valerolactone

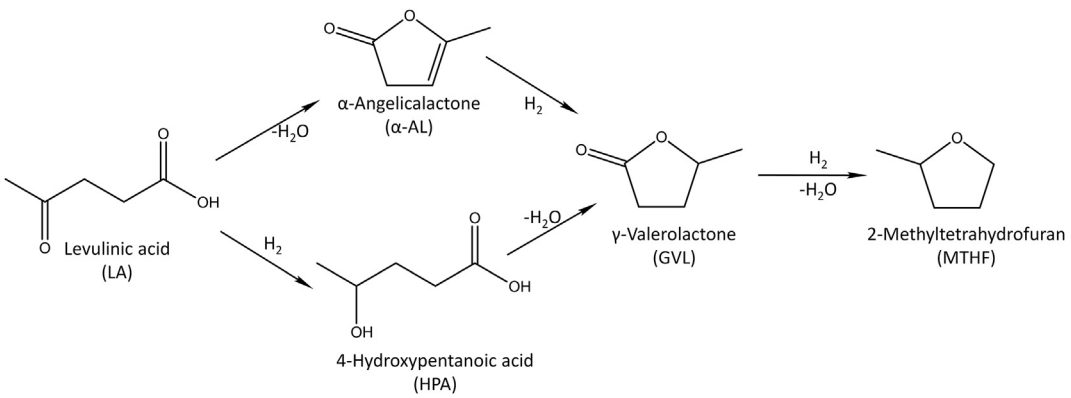

Scheme 1. Hydrogenation of LA to GVL with HPA and/or α-AL as the possible intermediate and MTHF as the over-hydrogenation product.

(MeMBL; an acrylic monomer) [13]), biofuels (e.g., 2-methyltetrahydrofuran (MTHF), valeric esters and alkane fuels) and specialty chemicals (e.g., adipic acid, caprolactone and 5-nonanone) [7]. Depending on the catalyst and reaction conditions, the synthesis of GVL from LA is typically performed via α-angelicalactone (α-AL; by the dehydration of LA) or 4-hydroxypentanoic acid (HPA; by the hydrogenation of LA) as the intermediate (Scheme 1). GVL can be further over-hydrogenated towards MTHF.

Molecular H_2 is typically utilized as the reducing agent, although the use of other (liquid phase) hydrogen donors like formic acid has also been reported [14]. The hydrogenation of LA is commonly performed over heterogeneous catalysts [15–18]. Noble metal catalysts, with Ru in particular, have received much research attention due to the high selectivity towards GVL (i.e., in several cases up to 100%) and good catalyst stability [19–22]. A variety of catalyst supports have been used for the immobilization of Ru (e.g., carbon, alumina, titania, zirconia) [23]. Ru supported on carbon (Ru/C) has the advantage of high specific catalyst surface area and is thus used extensively in the hydrogenation of LA to GVL [20,23–27], and many other hydrogenation reactions [28–32]. The Ru/C catalyzed hydrogenation of LA to GVL is often conducted with water as the solvent, although organic solvents have also been used (e.g., GVL [9], methanol [20], 1,4-dioxane [13,21,23–25], tetrahydrofuran (THF) [24]). GVL was used as the solvent for its own synthesis by the hydrogenation of LA (extracted from a water phase) over a Ru-Sn/C catalyst [9]. 1,4-Dioxane has similar properties to GVL and is thus often used as a mimic solvent for research purposes to facilitate GVL product quantification [13,23–25]. However, the toxicity of 1,4-dioxane makes it a less attractive solvent for industrial applications. The use of organic solvents with low boiling points (like THF, methanol) instead of water for LA hydrogenation can facilitate the product retrieval (e.g., due to energy saving in the downstream distillation) without wastewater generation [33].

The Ru/C catalyzed hydrogenation of LA to GVL has been performed in continuous flow reactors (e.g., packed bed milli-reactors) for catalyst stability testing [19,22], along with several studies in batch reactors to obtain mechanistic or kinetic insights [26,27,34]. The Ru/C catalyzed LA hydrogenation is generally considered 0.5th order in H_2 and zero order in the LA substrate [26,27]. This was also observed in the hydrogenation of glucose to sorbitol [32] and of alkyl levulinates to GVL [31]. In the latter case, a 1st order dependency in the substrate was observed at relatively low initial substrate concentrations (0.03–0.15 M) in methanol [31]. Piskun *et al.* found that in batch reactors (operated at 30–60 bar and 343–403 K) with water as the solvent, the 5 wt% Ru/C catalyzed hydrogenation of LA to GVL was partly limited by intraparticle mass transfer [27]. The Weisz-Prater numbers, calculated as the ratio between the experimentally observed reaction rate and the rate of internal diffusion [35], indicated that diffusion limitations occurred within the catalyst pores. These (intraparticle) mass transfer limitations of both hydrogen and LA were also observed in a packed bed milli-reactor [22], especially due to the larger catalyst particles used therein.

Dedicated studies focusing on reactor engineering aspects (e.g., in terms of the effect of reactor type and operating conditions on gas–liquid–solid mass transfer characteristics) for the optimization of reactor performance in the (Ru/C catalyzed) hydrogenation of LA are not widely performed to this date. The use of conventional gas–liquid–solid (e.g., batch, packed bed, slurry) reactors may not be promising in optimization primarily due to a limited control over the three-phase contact and heat or mass transfer thereof. In this respect, process intensification methods for gas–liquid–solid reactions have been developed. Particularly, continuous flow microreactors have received much research interest [36]. Microreactors allow multiphase operation under well-defined flow patterns (e.g., gas–liquid or liquid–liquid slug flow) that facilitate to investigate reaction kinetics and mass transfer characteristics thereof [37]. Due to their small internal channel sizes (i.e., diameter on the order of ca. 1 mm or below), microreactors offer several fundamental advantages (e.g., enhanced heat/mass transfer and reduced safety risks) [37,38]. The enhanced mass transfer in microreactors makes them interesting for multiphase reactions that tend to be limited by the species transport in (either of) the multiple phases, which is the case particularly when the intrinsic kinetic rate is relatively fast [39]. Furthermore, the superior heat transfer capability in microreactors, as well as the small lateral channel dimensions, allows safer operation by the precise temperature control and reduced explosion risk (e.g., in the case of strongly exothermic reactions or operation in the explosive regime) [40,41]. These merits are advantageous for hydrogenation reactions that often require high pressure operation to improve mass transfer (e.g., given low hydrogen solubility in the reaction solvent) and fine temperature control to avoid the hotspot formation in the reactor leading to runaway. Solid catalysts for such reactions can be also well handled in microreactors and are usually incorporated as wall-coatings or as small particles in a packed bed configuration [42–44]. To the best of the authors' knowledge, only one report dealt with the LA hydrogenation to GVL in microreactors [45]. Herein, the reaction was performed with formic acid as the hydrogen donor in water/methanol. A stainless steel capillary microreactor was wall-coated with silver/palladium nanoparticles supported on graphited carbon nitride ($AgPd/g\text{-}C_3N_4$). In a 50 min residence time at 70 °C, 100% GVL yield was obtained. The immobilization of solid catalysts onto a microreactor wall often requires tedious coating procedures and the catalyst replacement (i.e., in the case of irreversible catalyst deactivation or reactor malfunctioning) may require energy intensive procedures [38,46,47]. An alternative and more convenient way is by loading small catalyst particles to an empty microchannel (e.g., by gravitational or vacuum filling). Catalyst particles can then be held in place by filters or small inert particles (e.g., glass beads) to form a packed bed configuration [48–50]. This allows the direct use of commercial or laboratory-prepared catalysts (sometimes particle sieving or shaping is needed for compatibility with the microchannel dimension).

Although gas–liquid flow characteristics have been widely examined in conventional macroscale packed bed reactors [51], hydrodynamics in packed bed microreactors are not widely reported yet [49,50,52–59]. The dominance of surface forces over gravitational forces on the micrometer scale results in new gas–liquid flow features in packed bed microreactors [44]. A hydrodynamic study during the benzyl alcohol oxidation reaction in a packed bed microreactor (containing 1 wt% $Au\text{-}Pd/TiO_2$ catalyst) revealed two major gas–liquid flow patterns including the liquid-dominated slug flow and gas-continuous flow [58]. The liquid-dominated slug flow is similar to the induced pulsing flow in conventional large-scale packed bed reactors, and the gas-continuous flow to the trickle flow [58]. The transition from the liquid-dominated slug flow to gas-continuous flow was found to take place at a much smaller liquid to gas flow ratio than that observed in conventional packed bed reactors, due to the dominance of surface forces in packed bed microreactors. This transition further depends on several other factors such as the upstream gas–liquid flow pattern before entering the bed, particle size, shape and configuration, and the channel to particle diameter ratio [44].

Packed bed microreactors offer a better radial heat transfer than conventional (milli-scale or larger) packed beds, thus suppressing effectively the formation of hot spots and/or the explosion risks [44]. Higher gas–liquid–solid mass transfer rate is also attainable in packed bed microreactors due to smaller particles accommodated [50,60]. Thus, gas–liquid hydrogenation reactions in packed bed microreactors have gained increased research attention over the past decade [36,50,61–66]. In some cases, mass transfer limitations were (almost) eliminated and the reactions were under kinetic control, making packed bed microreactors a promising tool for kinetic investigations [61,63,64].

In this work, the hydrogenation of LA was performed in capillary microreactors made of perfluoroalkoxy alkane (PFA) packed with 0.5 wt% Ru/C as the solid catalyst. Molecular H_2 was used as the gas

phase and 1,4-dioxane as the organic solvent. The effect of various operating parameters in the packed bed microreactor (e.g., flow rate and ratio, temperature, pressure, catalyst particle size and concentration) on the reaction performance (in terms of the LA conversion and GVL yield) was investigated. A microreactor model was subsequently developed to describe the experimental results and to further identify the rate limiting steps (i.e., gas–liquid mass transfer, external or internal liquid–solid mass transfer, or kinetics). Finally, with the developed model, directions for further reaction optimization in the microreactor could be established.

2. Experimental

2.1. Materials and chemicals

Levulinic acid (> 98%) and γ-valerolactone (> 98%) were obtained from Acros Organics, 1,4-dioxane (> 99%) and dodecane (> 99.5%) from TCI Europe N.V., 2-methyltetrahydrofuran (> 99%), α-angelicalactone (98%), D_2O (99.9%) and SiC particles (with an average diameter of 0.48 mm) from Sigma-Aldrich and 0.5 wt% Ru/C catalyst particles (surface area of ca. 1000 m^2/g) from Strem Chemicals. The catalyst particles were ground and sieved into different size fractions before use (with an average particle diameter (d_p) being ca. 0.3 or 0.45 mm). H_2 and N_2 gases were obtained from Linde Gas (99.9%).

2.2. Setup and procedure

Reactions were performed in a Microactivity Effi reactor from PID Eng&Tech (Fig. 1). The liquid solution, consisting of 5–10 wt% LA and 1 wt% dodecane (*in situ* internal standard) in the 1,4-dioxane solvent, was fed at an inlet flow rate ($Q_{L,0}$) of 0.05–0.17 mL/min by a Williams piston pump (model P250 V225) to a stainless steel T-junction (0.75 mm bore size). H_2 or N_2 gas (supplied from a gas cylinder) was regulated by a mass flow controller (MFC) from Bronkhorst (EL-FLOW Select F-211CV) at an inlet gas flow rate ($Q_{G,0}$; i.e., at room temperature and reactor pressure) ranging from 0.16 to 0.33 mL/min. The gas and liquid feeds were guided through separate polytetrafluoroethylene (PTFE) capillaries (inner diameter: 0.8 mm; length: ca. 50 cm) that were preheated in an oven operated at a temperature of 70–130 °C. An upstream gas–liquid slug flow was then generated by mixing both feeds in a transparent PTFE capillary (inner diameter: 0.8 mm) for flow visualization. This was then connected to capillary microreactors (with inner diameter of d_C = 1.6 mm) made of PFA, packed with 0.5 wt% Ru/C catalyst particles (weight (w_c) of 0.45–0.9 g) by gravitational filling. During the filling procedure, the PFA capillary was frequently tapped to ensure a dense and reproducible packing state. Packed beds with lengths (L_{bed}) of 0.4–0.8 m were used in a vertical configuration where the gas–liquid mixture was introduced at the top to realize a downward flow. Polyether ether ketone (PEEK) connectors containing filters (75 µm mesh) made of PTFE and chlorotrifluoroethylene (CTFE) were incorporated at the in- and outlet of the bed to keep the packing in place. In some experiments, an additional PFA capillary, packed with inert SiC particles, was placed in front of the packed bed microreactor to generate an upstream slug flow with shorter gas bubbles and liquid slugs. The outlet of the microreactor was connected to a PTFE capillary (inner diameter: 0.8 mm) and directed towards a liquid level indicator/controller (LIC) where the gas and liquid phases were separated. The separator consisted of a capacitive level sensor with a very low dead volume [67]. This separation was regulated by a needle valve (i.e., controlled by the Effi operating system; Fig. 1) in the liquid outlet. The pressure (p) of the outlet gas stream was maintained at 9–15 bar with a pressure control valve located after the gas–liquid separator, after which it was exhausted to the fume hood. This valve was operated by the Effi, based on the measured pressure at the gas outlet by a pressure transducer from Sensor-Technik Wiedemann GmbH (model A09). The gas–liquid flows at the inlet (after the T-junction) and outlet (before the gas–liquid separator) of the packed bed microreactor were passed through a six-way valve. This pneumatic valve (controlled by an electrovalve) could be operated in two different positions: i) passing the gas–liquid stream through the packed bed and ii) directing the gas–liquid inlet flow immediately towards the gas–liquid separator and thus bypassing the microreactor (Fig. 1). Photos of the packed bed microreactor and slug flow profiles (both upstream and downstream; at room temperature and using N_2 as the inert gas instead of H_2) are also shown in Fig. 1, which were taken by a Nikon D3300 digital camera equipped with a Nikon lens (AF-S Micro Nikkor 60 mm f/2.8 G ED). Note that an isothermal microreactor operation is assumed in this work, given the preheating of the feeds, the insignificant reaction heat released (e.g., the estimated adiabatic temperature rise being around 7 °C for 5 wt% LA concentration at inlet; calculation details not shown for brevity) and

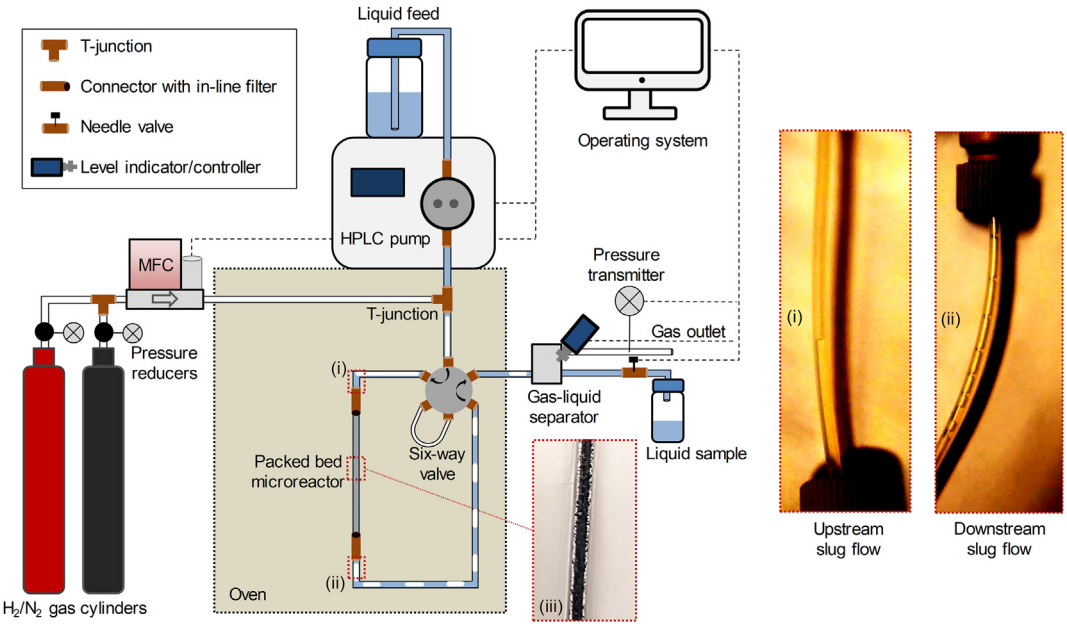

Fig. 1. Schematic representation of the experimental setup with pictures of (i) the upstream and (ii) the downstream gas–liquid slug flow profiles and (iii) the packed bed microreactor.

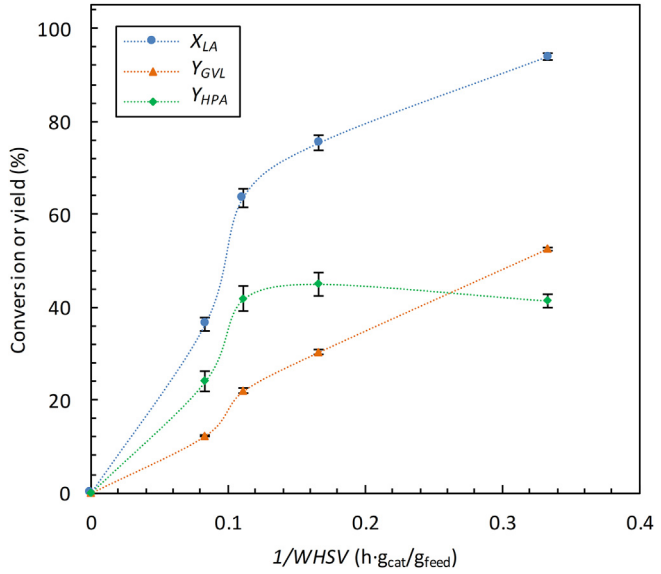

Fig. 2. Influence of the inverse weight hourly space velocity (1/*WHSV*) on the measured LA conversion, GVL and HPA yields at the outlet of the packed bed microreactor. The values at $1/WHSV = 0$ correspond with the microreactor inlet. Conditions: $C_{LA,0}$ = 5 wt%, $Q_{G,0}/Q_{L,0}$ = 4.5, 12 bar H_2, 130 °C, L_{bed} = 0.8 m, w_c = 0.9 g, d_p = 0.45 mm. Lines are solely for illustrative purposes. Error bars above and hereafter represent the standard deviation based on at least three measurements at different times on stream under steady state conditions.

the fast heat transfer of the microreactor.

Liquid samples were collected every 20 min time on stream and prepared for gas chromatography and/or ^{1}H NMR analysis. The experimental data presented in this work are based on the measured sample concentrations under steady state conditions. Steady state was achieved once the measured concentration at the microreactor outlet did not alter for a given time on stream, which was usually after ca. 60 min (cf. Section S1 in the Supplementary Material). This relatively long time required is mainly due to the large empty volume (i.e., between the microreactor and the gas–liquid separator) of the system and the low flow rates used.

2.3. Analysis

The LA and GVL concentrations in the liquid samples were analyzed by gas chromatography with a Restek Stabilwax-DA column (30 m × 0.32 mm × 1 μm) equipped with a flame ionization detector (GC-FID). GC-samples were prepared by diluting 0.2 mL of the reaction mixture (i.e., collected from the liquid sample vessel; cf. Fig. 1) or the liquid feed with ca. 1.8 mL 1,4-dioxane. The temperature of the column was increased from 60 °C to 250 °C at 20 °C/min and held at 250 °C for 2 min. Helium was used as the carrier gas at 2.5 mL/min. For all experiments the relative error in the measured LA and GVL concentrations was found below 10%.

The molar ratios of LA, HPA and GVL in the above prepared analytic sample mixture were determined by ^{1}H NMR (300 MHz operated at 25 °C). One drop of such sample mixture was mixed with approximately 1 mL D_2O. The molar ratio of each species in the mixture was determined from the ratio of the respective NMR peak heights (2.1 ppm for LA, 1.03 ppm for HPA, and 1.3 ppm for GVL; cf. Supplementary Material, Section S1).

2.4. Definitions

The LA conversion (X_{LA}), GVL yield (Y_{GVL}) and selectivity (σ_{GVL}) are determined as follows

$$X_{LA} = \left(1 - \frac{C_{LA,1}}{C_{LA,0}}\right) \times 100\% \quad (1)$$

$$Y_{GVL} = \frac{C_{GVL}}{C_{LA,0}} \times 100\% \quad (2)$$

$$\sigma_{GVL} = \frac{Y_{GVL}}{X_{LA}} \times 100\% \quad (3)$$

where $C_{LA,0}$ and $C_{LA,1}$ are LA concentrations at the microreactor inlet and outlet, respectively. C_{GVL} is the concentration of GVL at the microreactor outlet.

The weight hourly space velocity of the liquid phase (*WHSV*; in $g_{feed}/(g_{cat}\cdot h)$) is defined as

$$WHSV = \frac{m_L}{w_c} \quad (4)$$

where m_L is the liquid mass flow rate.

The void fraction in the packed bed microreactor (ε) is determined by

$$\varepsilon = 1 - \frac{w_c}{V_{bed}\rho_S} \quad (5)$$

where ρ_S is the average density of the solid (catalyst) particles and V_{bed} is the bed volume.

3. Results and discussion

3.1. Mass balance and reaction profile

A typical reaction profile for the hydrogenation of LA to GVL is depicted in Fig. 2. The reaction was performed in the packed bed microreactor with a fixed length (L_{bed} = 0.8 m), where the weight hourly space velocity (*WHSV*; Eq. (4)) was varied by adjusting the total flow rate ($Q_{tot;} = Q_G + Q_L$, where Q_G and Q_L are the respective gas and liquid flow rates under the reaction temperature and pressure without consideration of the flow rate change due to reaction consumption) while the inlet gas to liquid volumetric flow ratio ($Q_{G,0}/Q_{L,0}$) was kept equal. Note that the pressure drop in the packed bed microreactor estimated according to the literature [59] was found insignificant compared to the total pressure applied. The results at $WHSV$ = 6.0 $g_{feed}/(g_{cat}\cdot h)$ are used as the benchmark conditions throughout this work ($C_{LA,0}$ = 5 wt%, $Q_{G,0}/Q_{L,0}$ = 4.5, 12 bar H_2, 130 °C, L_{bed} = 0.8 m, w_c = 0.9 g, d_p = 0.45 mm). Only the LA and GVL concentrations at the microreactor outlet could be determined quantitatively by GC-FID. The GVL yield (Eq. (2)) was consistently lower than the LA conversion (Eq. (1)), indicating that the reaction was not fully selective towards GVL and a closed mass balance could not be obtained by GC-FID analysis alone (Fig. 2). The gap in the mass balance was attributed to the HPA intermediate that could not be measured quantitatively by GC-FID. HPA could be detected by ^{1}H NMR, from which the molar ratios of LA, GVL and HPA in the reaction mixture were determined. These ratios, combined with the measured LA and GVL concentrations, resulted in nearly closed mass balances (cf. Section S1 in the Supplementary Material for more detailed explanation). As such, the HPA yield was determined from the LA conversion and GVL yield, assuming a 100% total selectivity towards HPA and GVL. This was further proven by the fact that alternative reaction products (i.e., MTHF and α-AL; cf. Scheme 1) were neither detected by GC nor ^{1}H NMR. For the over-hydrogenation of GVL towards MTHF, it is expected that much higher temperature/pressure and longer residence times are required. For instance, it has been reported that no GVL conversion was found after 4 h at 130 °C and 100 bar H_2 for the solvent-free conversion of GVL over 5 wt% Ru/C [68]. Also by using GVL (with an initial concentration of $C_{GVL,0}$ at 5 wt %) instead of LA as the substrate under otherwise the same benchmark conditions shown above, no appreciable decrease (< 5%) in the GVL concentration and no MTHF formation was observed at the

microreactor outlet, implying that the further hydrogenation of GVL did not occur (at a noteworthy rate) under the reaction conditions tested.

As Fig. 2 reveals, the measured LA conversion and GVL yield increased with increasing 1/*WHSV* (i.e., decreasing *WHSV*; translated into the prolonged residence time in the bed of a fixed length). Significant amounts of HPA (ca. 20–45% yield) were formed at a relatively low *WHSV* (i.e., up to 2.5 $g_{feed}/(g_{cat}\cdot h)$) under the reaction conditions used. This shows that the formation of HPA from LA is faster than the subsequent formation of GVL from HPA (Scheme 1). Only when the majority of LA was converted, the HPA yield started to decline because of its further conversion towards GVL. The abundant formation of HPA is probably because the lactonization of HPA to GVL under such

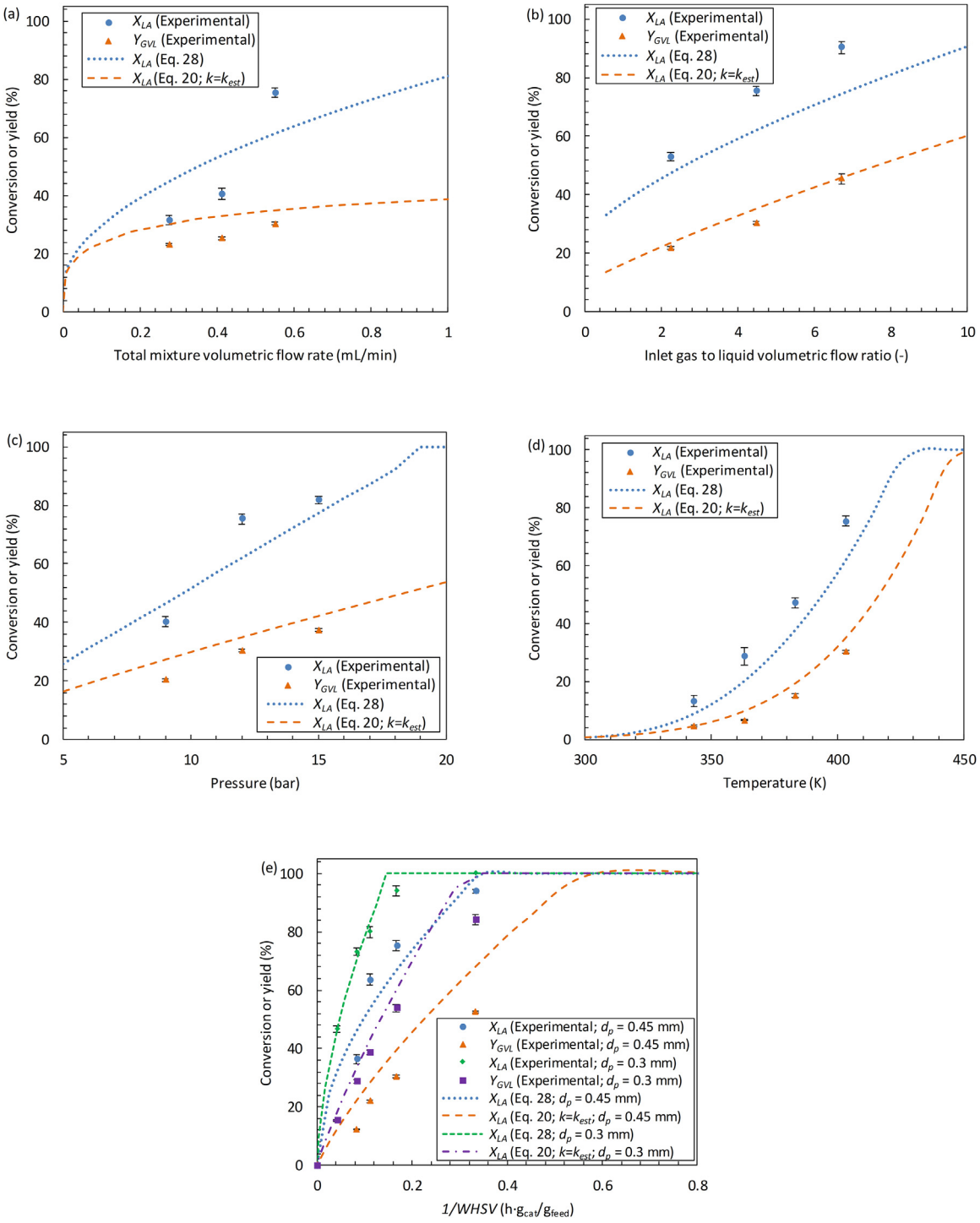

Fig. 3. Influence of reaction parameters on the measured LA conversion and GVL yield in the microreactor. (a) Influence of total mixture flow rate (Q_{tot}) under equal *WHSV* by varying the bed length (L_{bed} = 0.4–0.8 m) and thus the catalyst weight (w_c = 0.45–0.9 g), (b) influence of the inlet gas to liquid volumetric flow ratio (*WHSV* = 3–9 $g_{feed}/(g_{cat}\cdot h)$), (c) influence of pressure, (d) influence of temperature and (e) influence of catalyst particle size (L_{bed} = 0.75 mm for 0.3 mm diameter particles). Conditions (unless stated otherwise): $C_{LA,0}$ = 5 wt%, $Q_{G,0}/Q_{L,0}$ = 4.5, 130 °C, 12 bar H_2, L_{bed} = 0.8 m, w_c = 0.9 g, *WHSV* = 6.0 $g_{feed}/(g_{cat}\cdot h)$, Ru/C catalyst particle size (d_p) at 0.45 mm. The modeled LA conversions are shown for comparison, according to Eq. (28) (assuming the reaction rate was fully determined by the gas–liquid and external liquid–solid mass transfer of H_2) and Eq. (20) (based on a zero order in LA and 0.5th order in H_2; with the effectiveness factor calculated with Eq. (16) and the overall reaction rate constant (k) assumed equal to the estimated one (k_{est}) from the data of Ftouni *et al.* [24]).

relatively low temperature level is the rate limiting step (Scheme 1) [25]. This was also observed under similar reaction conditions in batch experiments performed at 373 K using 1,4-dioxane as the solvent and Ru/ZrO_2 as the catalyst [25], where the HPA intermediate was formed abundantly due to its relatively slow transformation towards GVL under not strongly acidic conditions.

The LA conversion and GVL yield were almost identical when performing the reaction in several microreactors with separate packings under the same operating conditions. This confirms that the packing methodology and experimental procedure were highly reproducible (cf. Supplementary Material, Section S2).

3.2. Influence of operating variables on the reaction performance

Several operation conditions were varied in the packed bed microreactor to investigate their influence on the mass transfer characteristics and reaction rate during LA hydrogenation over Ru/C. An initial LA concentration of 5 wt% was used in the majority of experiments. A few additional experiments were conducted with 10 wt% LA, which resulted in a lower LA conversion and GVL yield implying that the apparent LA consumption rate in the microreactor is below first order in LA (cf. Section S3 in the Supplementary Material for a more detailed explanation). The influence of gas–liquid flow behavior (i.e., total flow rate and gas to liquid flow ratio), H_2 pressure, reaction temperature and catalyst particle size on the measured LA conversion and GVL yield at the outlet of the packed bed microreactor is presented in Fig. 3. The selectivity towards GVL is on the order of ca. 40–60% for most experiments depicted (i.e., in the case of not all LA being consumed).

Influence of flow rate. The total mixture flow rate was altered (Q_{tot} = 0.27–0.55 mL/min) at a fixed inlet gas to liquid volumetric flow ratio ($Q_{G,0}/Q_{L,0}$ = 4.5). The *WHSV* was kept equal by varying the total mixture flow rate proportionally with the bed length (L_{bed} = 0.4–0.8 m) or alternatively the total catalyst weight in the bed (w_c = 0.45–0.9 g; particle size being ca. 0.45 mm). For a given *WHSV*, both the LA conversion and GVL yield increased with the increasing flow rate (Fig. 3a). Since parameters that could affect the intrinsic kinetic rate (i.e., temperature, concentrations of reactants, *WHSV* and gas–liquid flow ratio) were not changed, the observed difference in the reaction performance strongly indicates mass transfer limitations at lower flow rates. In other words, operation at higher flow rates would positively affect the gas–liquid [50,69,70] and liquid–solid [71,72] mass transfer coefficients in packed bed microreactors, therewith improving the overall reaction rate (in terms of the increased conversion and yield) if the intrinsic kinetic rate is relatively fast.

Influence of gas to liquid flow ratio. The inlet gas to liquid volumetric flow ratio was varied ($Q_{G,0}/Q_{L,0}$ = 2.24–6.71) by keeping the total mixture flow rate equal (Q_{tot} = 0.55 mL/min), the bed length being unchanged at 0.8 m (with a catalyst weight of 0.9 g). The measured LA conversion and GVL yield increased with the increasing gas to liquid flow ratio (Fig. 3b). Although the gas–liquid and external liquid–solid mass transfer coefficients in packed bed (micro)reactors are (slightly) affected by $Q_{G,0}/Q_{L,0}$ under otherwise the same reaction conditions [50,69–72], the main reason is probably that this ratio increase negatively affected the weight hourly space velocity of the liquid phase (*WHSV* = 3 or 9 $g_{feed}/(g_{cat}{\cdot}h)$ for $Q_{G,0}/Q_{L,0}$ of 6.71 or 2.24, respectively). In other words, there was more catalyst available for the conversion of LA at an increased $Q_{G,0}/Q_{L,0}$, resulting in a higher LA conversion (and GVL yield) at the reactor outlet under such conditions.

Influence of H_2 pressure. The H_2 pressure was varied while keeping other reaction conditions unchanged (Fig. 3c). A higher H_2 pressure resulted in a somewhat linear increase in the LA conversion and GVL yield (Fig. 3c). The increased H_2 pressure enhanced the liquid phase H_2 concentration which in turn positively affected the transfer rate of H_2 to the catalyst, or more specifically, increased the H_2 concentration over the catalyst external surface and thus the kinetic reaction rate (when the reaction is above zero order in H_2). As a result, the apparent reaction rate would increase with increased H_2 pressure.

Influence of reaction temperature. An increase in the reaction temperature, under otherwise unchanged conditions, resulted in a remarkable increase in the LA conversion and GVL yield (Fig. 3d). The temperature increase not only enhanced the intrinsic kinetic rate significantly according to the Arrhenius equation, but also improved to some extent the mass transfer rate of H_2 given the increased diffusion coefficient and solubility of H_2 in the liquid phase (i.e., 1,4-dioxane) [73]. The latter mass transfer rate enhancement also contributed to the observed LA conversion or GVL yield increase as is better explained in the modeling section (cf. Section 3.5).

Influence of catalyst particle size. Reactions were performed in packed bed microreactors with two different catalyst particle sizes (diameter of ca. 0.45 and 0.3 mm) (Fig. 3e). The same catalyst weight was used and the resulted length of the packed bed microreactor was almost equal (L_{bed} = 0.8 m and 0.75 m for d_p = 0.45 and 0.3 mm, respectively) given no order-of-magnitude difference in the particle diameter, so that the void fraction (ε) was nearly equal (Eq. (5)). The LA conversion and GVL yield were significantly higher for a certain *WHSV* when using smaller catalyst particles (Fig. 3e), where 100% LA conversion and 84% GVL yield were obtained at 130 °C, 12 bar H_2 and a *WHSV* of 3.0 $g_{feed}/(g_{cat}{\cdot}h)$. It is commonly known that the use of smaller particles significantly enhances the specific catalyst area, therewith increasing the external liquid–solid H_2 transfer rate [22,27]. Furthermore, the internal diffusion of both H_2 and LA within smaller particles tends to be improved [27]. Thus, the increase in the overall reaction rate observed here with smaller particle sizes is an additional indication of the presence of liquid–solid mass transfer limitations.

3.3. Comparison with literature results

The measured microreactor performance is further compared with the literature results, where a weight hourly space velocity of the LA itself ($WHSV_{(LA)}$; in $g_{LA}/(g_{cat}{\cdot}h)$) was recalculated in order to account for the LA concentration difference in all works (Table 1). The value of $WHSV_{(LA)}$ was estimated for packed bed reactors or microreactors from

Table 1
Comparison of Ru/C catalyzed hydrogenation of LA to GVL in different reactor configurations.

Reactor	Ru/C (wt%)	d_p (mm)	Solvent	$WHSV_{(LA)}$ ($g_{LA}/(g_{cat}{\cdot}h)$)	T [c] (°C)	p_{H_2} [d] (bar)	X_{LA} (%)	Y_{GVL} (%)	Reference
MR [a]	0.5	0.3	dioxane	0.15	130	12	100	84	This work
Batch	5	–	dioxane	2.1	100	30	–	97	[24]
Batch	5	–	dioxane	16.7	150	30	–	99	[24]
Batch	3	0.06	water	50	130	45	97	88	[27]
PBR [b]	0.5	1.88	water	4.15	130	45	99	–	[22]

[a] Microreactor (d_C = 1.6 mm).
[b] Packed bed reactor (6 mm inner diameter).
[c] Reaction temperature.
[d] H_2 pressure.

the division of the inlet mass flow rate of LA by the packed catalyst weight, and for batch slurry reactors from the initial mass of LA divided by the product of the suspended catalyst weight and the batch reaction time.

In the current microreactor (d_C = 1.6 mm and L_{bed} = 0.75 m) with 1,4-dioxane as the solvent, a best GVL yield of 84% was obtained at 100% LA conversion over the 0.3 mm diameter particles of Ru/C catalyst under a weight hourly space velocity of the liquid phase (*WHSV*) of 3.0 $g_{feed}/(g_{cat}·h)$ (corresponding to $WHSV_{(LA)}$ = 0.15 $g_{LA}/(g_{cat}·h)$), 130 °C and 12 bar H_2. As Table 1 reveals, under similar reaction conditions (i.e., 100 or 150 °C, 30 bar H_2 and 1,4-dioxane as the solvent), nearly 100% GVL yield was obtained over 5 wt% Ru/C catalyst at a $WHSV_{(LA)}$ of 2.1 or 16.7 $g_{LA}/(g_{cat}·h)$ in a batch autoclave [24]. Performing the reaction with water as the solvent and otherwise similar reaction conditions in a batch setup (130 °C and 45 bar H_2) resulted in 97% LA conversion and 88% GVL yield over 3 wt% Ru/C catalyst at a $WHSV_{(LA)}$ of 50 $g_{LA}/(g_{cat}·h)$ [27], whereas a $WHSV_{(LA)}$ of 4.15 $g_{LA}/(g_{cat}·h)$ was required to achieve similar results in the milli-reactor packed with 0.5 wt% Ru/C at the same temperature and pressure [22]. The lesser performance in the latter case, in terms of a lower $WHSV_{(LA)}$ value required for a similar LA conversion, was probably due to the lower Ru loading and the much larger catalyst particles used (d_p = 1.88 mm vs. 60 μm in the batch autoclave), which caused liquid–solid mass transfer limitations that resulted in a slower reaction rate. In other words, batch reactors allow the use of finer catalyst particles than in packed bed reactors (i.e., due to otherwise the excessive pressure drop generated in the latter). As such, external and internal liquid–solid mass transfer limitations can be significantly improved or even overcome in batch reactors by the increased specific catalyst area and shorter diffusion distance within catalyst pores, therewith accelerating the reaction rate towards obtaining the intrinsic one. These would also largely explain the observed less satisfactory performance in the current packed bed microreactor compared with its batch counterparts. Despite the larger catalyst particles used in the milli-packed bed reactor [22], a better performance was found than the microreactor studied here. This may be attributed to the use of higher H_2 pressure and water as the solvent in the former case. The better reaction performance of water than 1,4-dioxane as the solvent was also seen in batch reactor studies [24,27], likely due to the solvent effect on the kinetic parameters. Besides that, H_2 has a higher solubility and diffusivity in water than in 1,4-dioxane [73–75], which positively affected both the H_2 mass transfer rate towards the catalyst internal surface and the kinetics (i.e., in the case the rate is above zero order in H_2).

3.4. Development of the microreactor model

To explain the observed reaction performance in the packed bed microreactor, the gas–liquid–solid contact behavior and the associated mass transfer characteristics, the intrinsic kinetics and their roles in determining the overall reaction rate need to be well understood. This eventually would lead to the establishment of a microreactor model that describes the LA hydrogenation results (especially in terms of the LA conversion) under steady state conditions and indicate the direction of improvement in the microreactor design and operation.

Gas-liquid flow pattern in the packed bed microreactor. From the respective gas and liquid superficial velocities (i.e., j_G and j_L) of experiments in this work, the gas–liquid flow pattern in the packed bed microreactor was predicted to be liquid-dominated slug flow based on the flow map proposed by Al-Rifai *et al.* [58] (Fig. 4). This flow map was derived based on their experiments with a square microreactor (width × height × length = 300 μm × 600 μm × 190 mm), packed with 1 wt% Au-Pd/TiO_2 catalyst (d_p = 65 μm) operated under an upstream slug or (wavy-)annular flow profile at 120 °C and 1 bar [58]. Thus, such flow map is expected applicable to a large extent in the current work, given similar inlet mixing conditions (i.e., an upstream gas–liquid slug flow profile) and value range of the microchannel diameter to particle ratio.

In the majority of our experiments, the upstream slug flow profile had relatively long gas bubbles and liquid slugs (Fig. 1). To test if this negatively affected the reaction performance, the upstream gas–liquid slug flow profile was further altered by placing a PFA capillary (inner diameter: 1.6 mm) packed with an inert bed of SiC particles (particle diameter: 0.48 mm; bed length: 10 cm) right after the stainless steel T-junction, by which significantly shorter bubbles/slugs were generated in the connected short PTFE capillary and subsequently fed to the packed bed microreactor. The change of the upstream slug flow profile did not have a considerable effect on the LA conversion and GVL yield for given reaction conditions (cf. Section S4 in the Supplementary Material for more details). Thus, it is concluded that even in the case of the relatively long bubbles/slugs in the upstream flow, the gas–liquid–solid contact pattern and the associated mass transfer in the packed bed microreactor are not much negatively affected. From this it is safely assumed that all experiments in this work were performed in the liquid-dominated slug flow regime, indicating a high liquid–solid interaction [58].

Mass transfer and reaction analyses in the packed bed microreactor. In the heterogeneously catalyzed hydrogenation of LA, H_2 is first transferred from the gas to the liquid phase, and then both LA and the dissolved H_2 travel towards the solid catalyst active sites. The microreactor model was therefore based on the mass transfer and reaction steps of H_2 and LA, consisting of (1) transfer of H_2 from the gas bulk to the gas–liquid interface and the subsequent H_2 absorption at the interface, (2) H_2 transfer from the liquid interface to the liquid bulk, (3) H_2/LA transfer from the liquid bulk to the external catalyst surface (3a and b) and finally (4) the internal diffusion of H_2/LA into the catalyst pores, with the reaction occurring on the catalytic surface of the pores (Fig. 5). The transfer rate for each individual step is estimated based on the literature (empirical) mass transfer or kinetic correlations. The physical fluid properties relevant to such estimation are given in Section S5 in the Supplementary Material.

The simplified mass transfer and reaction steps shown in Fig. 5 were applied to the microreactor cross-section at one axial location. This, combined with the estimated transfer rate of each step and the overall mass balance in the microreactor, finally resulted in a one-dimensional model (*vide infra*).

Gas-liquid mass transfer. Since pure H_2 gas was used, there were no

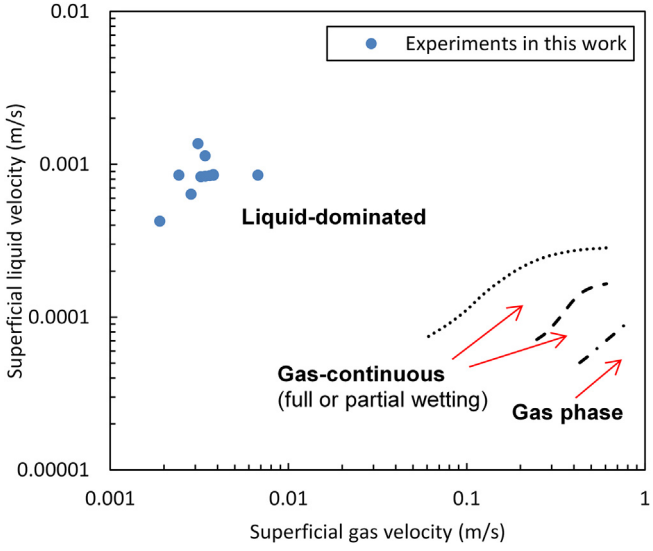

Fig. 4. Influence of the superficial gas and liquid velocities on the gas–liquid flow pattern in the packed bed microreactor. Lines depict the transition boundary between each flow pattern according to the experimental work of Al-Rifai *et al.* [58].

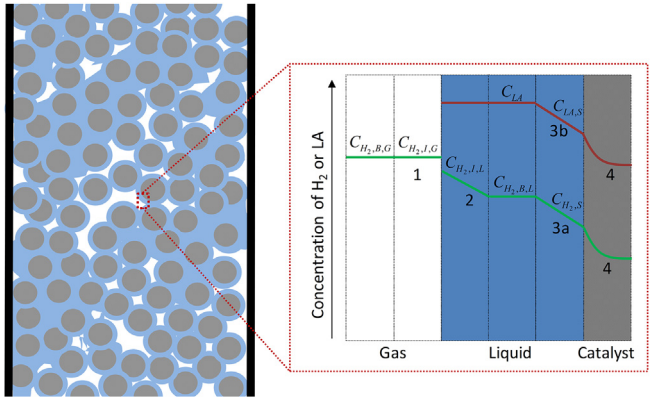

Fig. 5. Schematic overview of mass transfer and reaction steps for the heterogeneously catalyzed LA hydrogenation. (1) Transfer of H_2 from the gas bulk ($C_{H_2,B,G}$) to the gas-side interface ($C_{H_2,I,G}$) and its subsequent absorption at the interface. (2) H_2 transfer from the liquid-side interface ($C_{H_2,I,L}$) to the liquid bulk ($C_{H_2,B,L}$). (3a) H_2 diffusion from the liquid bulk to the catalyst external surface ($C_{H_2,S}$). (3b) LA diffusion from the liquid bulk (C_{LA}) to the catalyst external surface ($C_{LA,S}$). (4) Internal diffusion of H_2/LA into the catalyst particle surface, adsorption and reaction on the active site. The term in the above brackets designates the concentration of H_2 or LA at the respective location.

gas phase mass transfer limitations and the H_2 concentration in the gas bulk ($C_{H_2,B,G}$) is equal to the gaseous H_2 concentration at the interface ($C_{H_2,I,G}$). The liquid phase H_2 concentration at the interface ($C_{H_2,I,L}$) is thus derived as

$$C_{H_2,I,L} = \frac{C_{H_2,G}}{H} \tag{6}$$

where H is the Henry constant, determined from the solubility of H_2 in the 1,4-dioxane solvent (cf. Supplementary Material, Section S5.1) [73].

The transport rate of H_2 from the liquid interface to the liquid bulk ($r_{H_2,G-L}$) is described by

$$r_{H_2,G-L} = V_{bed} k_L a_i (C_{H_2,I,L} - C_{H_2,B,L}) \tag{7}$$

where k_L is the liquid phase mass transfer coefficient, a_i is the specific gas–liquid interfacial area (based on the total bed volume V_{bed}) and $C_{H_2,B,L}$ denotes the H_2 concentration in the liquid bulk.

The volumetric liquid phase mass transfer coefficient ($k_L a_i$) for packed bed microreactors is estimated by the empirical correlation proposed by Zhang *et al.* [69].

$$k_L a_i = \frac{3.41 \times 10^{-5} \chi_G^{0.08} Re_L^{3.1} We_L^{-1.33} D_{H_2}}{{d_p}^2} \tag{8}$$

where χ_G is the Lockhart-Martinelli ratio, Re_L and We_L are the Reynolds and Weber numbers of the liquid phase, respectively, and D_{H_2} is the mass diffusivity of H_2 in 1,4-dioxane (estimated by the Wilke-Chang correlation [75], see Section S5.2 in the Supplementary Material for calculation details). Eq. (8) was developed based on experiments with chemical absorption of CO_2 into the aqueous methyl diethanolamine solution under liquid-dominated slug flow through microreactors (inner diameter: 3.05–4.57 mm) packed with inert glass beads (particle size: 75–355 μm; bed length: 10 cm) [69], and is considered roughly applicable to describe $k_L a_i$ in the current microreactor system given more or less similar process parameters (e.g., gas–liquid flow regime, microreactor diameter and particle size range).

External liquid–solid mass transfer. The rates of H_2 and LA transfer from the liquid bulk to the external catalyst surface ($r_{H_2,L-S}$ and $r_{LA,L-S}$, respectively) are described by

$$r_{H_2,L-S} = \alpha w_c k_S a_c (C_{H_2,B,L} - C_{H_2,S}) \tag{9}$$

$$r_{LA,L-S} = \alpha w_c k_S a_c (C_{LA} - C_{LA,S}) \tag{10}$$

where k_S is the liquid–solid mass transfer coefficient and a_c the specific external surface area of the solid catalyst (based on the catalyst weight). $C_{H_2,S}$ and $C_{LA,S}$ are the H_2 and LA concentrations on the catalyst external surface, respectively. C_{LA} is the bulk liquid concentration of LA. α is the wetted fraction of the catalyst external surface. In the current work, α is taken as 1 given the presence of a good catalyst wetting in the involved liquid-dominated slug flow regime [58].

For spherical catalyst particles a_c is derived from

$$a_c = \frac{A_c}{V_c \rho_S} = \frac{\pi {d_p}^2}{\frac{\pi}{6} {d_p}^3 \rho_S} = \frac{6}{d_p \rho_S} \tag{11}$$

where A_c and V_c are the surface area and volume of the catalyst particles, respectively.

k_S can be obtained from the literature correlations for the Sherwood number (Sh) defined for packed bed (micro)reactors as

$$Sh = \frac{k_S d_p}{D_i} \tag{12}$$

Correlations for estimating Sh as a function of the conventional large packed bed reactor geometry and flow conditions are extensively reported, however, these are limited for packed bed microreactor configurations where the inner channel to particle diameter ratio (d_C/d_p) is generally low (e.g., being 3.55–5.33 in this work) [71,72]. According to Tidona *et al.* [71], Sh for (capillary) reactors with low values of d_C/d_p (< 6.6) is best described by the correlation of Wakao and Funazkri [76]:

$$Sh = 2 + 1.1 {Re_L}^{0.6} {Sc_L}^{1/3} \tag{13}$$

where Sc_L is the liquid phase Schmidt number.

According to Eq. (13), the liquid–solid mass transfer coefficient of H_2 ($k_S = 2.05 \times 10^{-5}$ m/s) is significantly lower than that of LA in 1,4-dioxane ($k_S = 7.13 \times 10^{-5}$ m/s) under the benchmark conditions in this work, mainly due to their different mass diffusivities in 1,4-dioxane (cf. Table S1 and Section S5.2 in the Supplementary Material for calculation details). Above that, the initial LA concentration ($C_{LA,0} = 0.44$ mol/L) in the liquid phase is far higher than that of H_2 (i.e., being 5.38×10^{-3} mol/L under the benchmark conditions; Eq. (6)). As such, the transfer rate of LA from the liquid bulk to the external catalyst surface is considered not limiting compared with that of H_2 (Eqs. (9) and (10)).

Internal liquid–solid mass transfer and kinetics. The H_2 internal diffusion within the catalyst particle pores is combined with surface reaction by using the concept of the effectiveness factor of the catalyst (η). The obtained actual rate of reaction ($r_{H_2,R}$) is described by

$$r_{H_2,R} = w_c \eta r'_{H_2,S} \tag{14}$$

where $r'_{H_2,S}$ is the surface kinetic reaction rate per unit mass of catalyst (in mol/(g_{cat}·s)).

The kinetics of the Ru/C catalyzed hydrogenation of LA has been described by a Langmuir-Hinshelwood mechanism [26,27], according to which the conversion of LA to HPA takes place on the catalyst surface by two subsequent half-hydrogenations (cf. the reaction equations S9-S12 in the Supplementary Material). Computational studies have suggested that the successive half-hydrogenation of the previously half-hydrogenated LA intermediate on the catalyst surface (LA-H*) is the rate limiting step [77]. When considering that the catalyst's active sites are far from being fully covered by H_2 with almost zero coverage of LA [26], the kinetic rate can be simply described as 0.5th order in H_2 and zero order in LA (cf. Supplementary Material, Section S6 for a more detailed explanation) [26,27]. Under such assumptions, Eq. (14) is rewritten as

$$r_{H_2,R} = w_c \eta k C_{H_2S}^{1/2} \tag{15}$$

This 0.5th order in H_2 and zero order in the liquid substrate (LA in this case) are often observed for gas–liquid–solid (Ru/C-catalyzed) hydrogenation reactions (e.g., glucose to sorbitol [32], cyclohexene to

cyclohexane [78]). So far, the detailed information of the overall reaction rate constant (k) related to LA or H_2 consumption is still not available for the current reaction system. Thus, it was roughly estimated from the reported batch studies by Ftouni *et al.* [24] on the 5 wt % Ru/C catalyzed hydrogenation of LA in 1,4-dioxane. Herein, their measured GVL yields at different reaction times and temperatures were used to obtain the estimated k value (referred to as k_{est}), based on the assumptions of a 100% selectivity to GVL as well as a 0.5th order in H_2 and a zero order in LA (cf. Supplementary Material, Section S7) [26,27]. This approach underestimates the actual k values since the LA conversion (not reported in their work) should be higher than the GVL yield to a certain extent because of the presence of HPA as the intermediate (e.g., at short reaction times). However, k_{est} is still expected to be around the same order of magnitude as the actual k value, which is sufficient to reveal the dominant role of mass transfer in the present microreactor experiments (*vide infra*). The k_{est} values at different reaction temperatures (323–423 K) were then used to derive the activation energy (E_a = 58 kJ/mol) and the pre-exponential factor (A = 1770 $(mol{\cdot}L)^{0.5}/(g_{cat}{\cdot}h)$), so that k_{est} could be estimated as a function of temperature with the Arrhenius equation. Albeit the rather approximate nature of this estimation, the obtained E_a value is close to that obtained in the cases of the hydrogenation of LA to HPA in water (E_a = 48 kJ/mol) [26] and hydrogenation of alkyl (i.e., methyl, ethyl and butyl) levulinates to their corresponding alkyl-3-hydroxyvalerates (i.e., the ethers of HPA; Scheme 1) in methanol (E_a = 41, 45 or 58 kJ/mol, respectively), both over 5 wt% Ru/C [31].

Effectiveness factors were estimated with the Thiele modulus (ϕ), that represents the ratio between the surface reaction rate (according to the kinetics) and the diffusion rate through the catalyst pores (cf. Section S8 in the Supplementary Material for calculation details). For low values of the Thiele modulus (e.g., $\phi < 0.2$), η approaches 1 and the internal diffusion is not rate-limiting. For larger values (e.g., $\phi > 15$), η is much smaller than 1 with the surface reaction being not rate limiting and its value for an n-th-order reaction over spherical catalyst particles is roughly estimated as [79]

$$\eta = \left(\frac{2}{n+1}\right)^{1/2}\frac{3}{\phi} \tag{16}$$

When assuming no concentration gradient of the other reacting component within the catalyst pores, the Thiele moduli were estimated as 31.0 for H_2 and 1.48 for LA under the benchmark conditions, corresponding to effectiveness factors of η_{H_2} = 0.11 (i.e., based on Eq. (16) with n = 0.5) and η_{LA} that can be assumed as 1 [79] (cf. Section S8 in the Supplementary Material for elaboration).

Overall reaction rate and LA conversion. At steady state conditions, $r_{H_2,G-L} = r_{H_2,L-S} = r_{H_2,R}$. Thus, the overall rate of H_2 consumption (r_{H_2}) is expressed by combining Eqs. (6), (7), (9) and (15) as

$$r_{H_2} = \frac{C_{H_2,G}/H}{\frac{1}{V_{bed}k_La_i} + \frac{1}{\alpha w_c k_S a_c} + \frac{r_{H_2}}{(w_c\eta k)^2}} \tag{17}$$

It is finally obtained that

$$r_{H_2} = \frac{-\left(\frac{1}{V_{bed}k_La_i} + \frac{1}{\alpha w_c k_S a_c}\right) + \sqrt{\left(\frac{1}{V_{bed}k_La_i} + \frac{1}{\alpha w_c k_S a_c}\right)^2 + \frac{4C_{H_2,G}}{H(w_c\eta k)^2}}}{\frac{2}{(w_c\eta k)^2}} \tag{18}$$

Given no occurrence of other hydrogenation reactions (e.g., the formation of MTHF), the rate of LA consumption (r_{LA}) is assumed equal to r_{H_2}. Since the reaction is zero order in LA, $r_{H_2,R}$ is not affected by the change in C_{LA} along the microreactor (Eq. (15)). Also, $C_{H_2,G}$ is constant as the gas phase consisted of pure H_2 and the pressure drop over the bed is not significant compared with the pressure applied (i.e., the partial H_2 pressure is approximately equal at the bed in- and outlet) [59]. Thus, r_{LA} is constant throughout the microreactor. The LA concentration at the outlet of the packed bed microreactor ($C_{LA,1}$) is then derived from the overall mass balance as

$$C_{LA,1} = C_{LA,0} - \frac{r_{LA}}{Q_{L,0}} = C_{LA,0} - \frac{r_{H_2}}{Q_{L,0}} \tag{19}$$

under the condition that $C_{LA,1} = 0$ when $C_{LA,0} \leqslant r_{LA}/Q_L$.

The modeled LA conversion is obtained by combining Eqs. (1), (18) and (19) as

$$X_{LA} = \frac{r_{LA}}{Q_{L,0}C_{LA,0}} = \frac{-\left(\frac{1}{V_{bed}k_La_i} + \frac{1}{\alpha w_c k_S a_c}\right) + \sqrt{\left(\frac{1}{V_{bed}k_La_i} + \frac{1}{\alpha w_c k_S a_c}\right)^2 + \frac{4C_{H_2,G}}{H(w_c\eta k)^2}}}{\frac{2Q_{L,0}C_{LA,0}}{(w_c\eta k)^2}} \tag{20}$$

GVL formation rate and yield. Conversion of HPA to GVL is considered via an equilibrium intramolecular esterification reaction (Scheme 1), catalyzed by a Brønsted acid (e.g., from the dissociation of LA and HPA) [26,27]. Thus, the reaction is expected to occur in the liquid bulk rather than at the catalyst surface. The GVL formation rate (r_{GVL}) is considered first order in both HPA and the acid (i.e., based on kinetic studies in water) [26,27]. That is,

$$r_{GVL} = k_2 C_{HPA} C_{H^+} - k_{-2} C_{GVL} C_{H^+} \tag{21}$$

where k_2 and k_{-2} are the respective reaction rate constants for the conversion of HPA to GVL and vice versa. C_{HPA} and C_{H^+} are the respective HPA and acid concentrations in the liquid bulk. The value of C_{H^+} can be estimated from the dissociation constants of LA and HPA in 1,4-dioxane (i.e., in the case of no other acid presence) [27].

In the current microreactor setup (Fig. 1), this HPA to GVL conversion presumably did not solely occur in the liquid contained in the catalyst bed, but also in the liquid segment present in the subsequent heated tubing sections between the bed outlet and the gas–liquid separator. For an accurate estimation of the GVL yield, the total liquid volume heated at the reaction temperature ($V_{L,tot}$) should thus be taken into consideration. The relation of the GVL formation rate and thus its yield as a function of $V_{L,tot}$ is then described as

$$Q_{L,0}\frac{dC_{GVL}}{dV_{L,tot}} = Q_{L,0}C_{LA,0}\frac{dY_{GVL}}{dV_{L,tot}} = r_{GVL} \tag{22}$$

Eqs. (21) and (22) do not consider the influence of mass transfer effects (e.g., HPA diffusion from the catalyst surface to the liquid bulk). Moreover, the kinetic parameters of the HPA lactonization to GVL in the 1,4-dioxane solvent are not available yet. Thus, the GVL yield is not dealt with in the current model.

3.5. Model discussion

The experimental LA conversion under the operating conditions was compared with the model prediction (Eq. (20); Fig. 3). The effectiveness factor was determined by Eq. (16) (for the case of zero order in LA and 0.5th order in H_2) and the kinetic constant was assumed equal to that estimated in Section S7 of the Supplementary Material ($k = k_{est}$). For each experimental condition the measured LA conversion was largely underestimated by Eq. (20) (Fig. 3). This is probably because k_{est} underestimates the actual k value, as already mentioned before. Despite this, the general trend could be followed by the model. An analysis over the different mass transfer and reaction steps was performed to unravel the reason for this underestimation. To investigate the individual contribution of reaction parameters to the different steps of H_2 transfer involved in the process (cf. Fig. 5), the respective resistances (in s/m^3) for the gas–liquid mass transfer of H_2 ($\Omega_{H_2,G-L}$), the external liquid–solid mass transfer of H_2 ($\Omega_{H_2,L-S}$), and the combined resistance for internal diffusion of H_2 and surface reaction ($\Omega_{H_2,R}$) were estimated according to the following relation [80]:

$$r_{H_2} = \frac{C_{H_2,G}/H}{\Omega_{H_2,G-L} + \Omega_{H_2,L-S} + \Omega_{H_2,R}} \tag{23}$$

These resistances are defined as

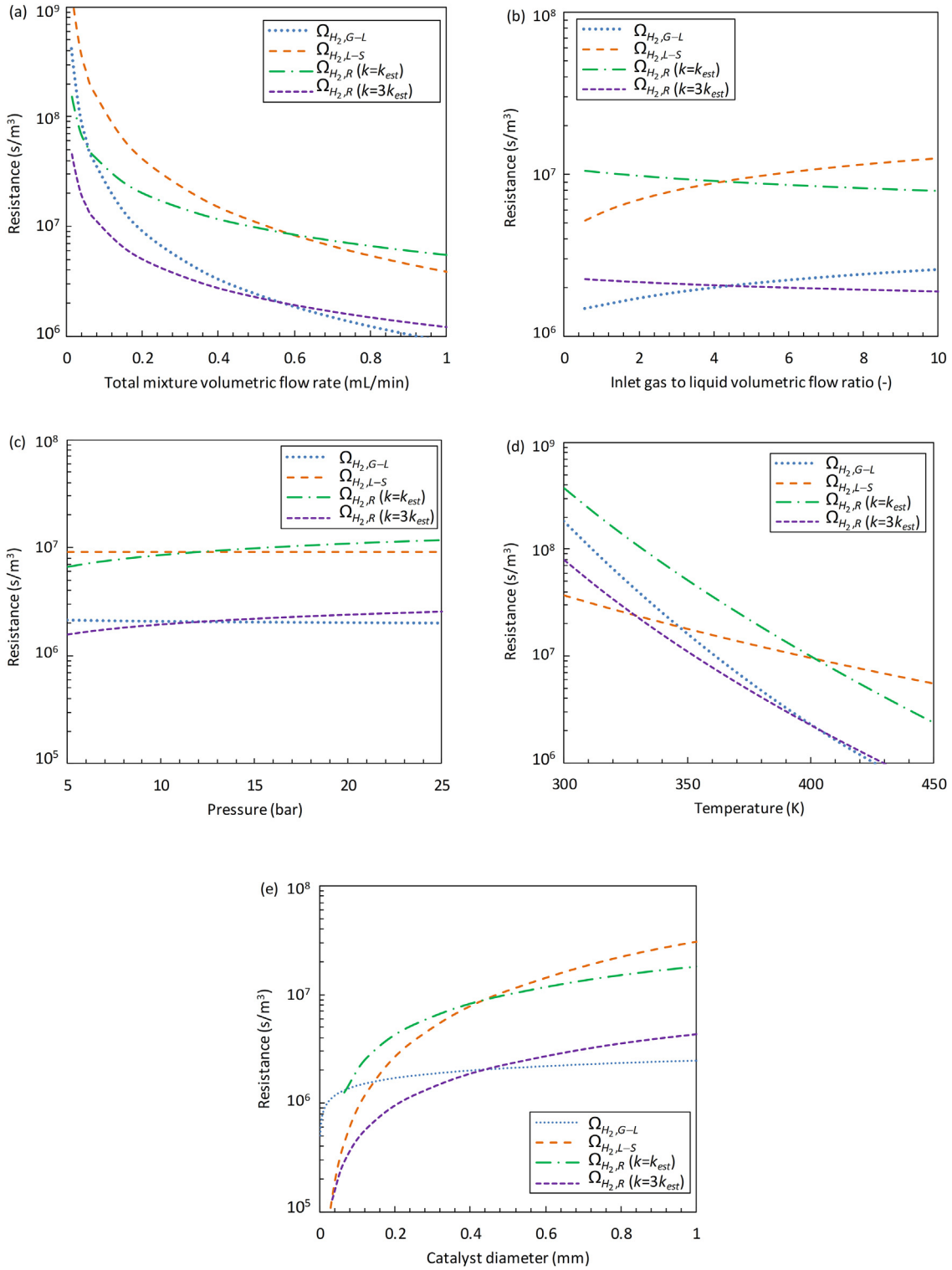

Fig. 6. Influence of reaction parameters on the different resistances (Ω; Eqs. (24)–(26)). Conditions (unless stated otherwise): $C_{LA,0}$ = 5 wt%, Q_{tot} = 0.55 mL/min, $Q_{G,0}/Q_{L,0}$ = 4.5, 130 °C, 12 bar H_2, L_{bed} = 0.8 m, w_c = 0.9 g, *WHSV* = 6.0 $g_{feed}/(g_{cat}·h)$, Ru/C catalyst particle size (d_p) at 0.45 mm. (a) Influence of the total volumetric flow rate (Q_{tot} = 0.007–1.0 mL/min) with equal *WHSV* and $Q_{G,0}/Q_{L,0}$, and varying bed length (L_{bed} = 0.01–2 m) and catalyst weight (w_c = 0.011–2.25 g), (b) Influence of gas to liquid volumetric flow ratio ($Q_{G,0}/Q_{L,0}$ = 0.4–10) corresponding to a *WHSV* between 2.71 and 21 $g_{feed}/(g_{cat}·h)$), (c) influence of pressure (5–25 bar), (d) influence of temperature (300–450 K) and (e) influence of catalyst particle size (d_p = 1 μm–1 mm). In the calculation of $\Omega_{H2,R}$ (Eq. (26)), the estimated k value ($k = k_{est}$) or a tripled value ($k = 3k_{est}$) was used.

$$\Omega_{H_2,G-L} = \frac{1}{V_{bed} k_L a_i} \quad (24)$$

$$\Omega_{H_2,L-S} = \frac{1}{\alpha w_c k_S a_c} \quad (25)$$

$$\Omega_{H_2,R} = \frac{r_{H_2}}{(w_c \eta k)^2} \quad (26)$$

A comparison of these resistances can give valuable insights in finding the rate limiting step under the tested reaction conditions and beyond, as shown in Fig. 6. Since k_{est} likely underestimates the actual kinetic constant, two k values were used in the comparison of $\Omega_{H_2,R}$. That is, the estimated kinetic constant ($k = k_{est}$) and a tripled value ($k = 3k_{est}$).

According to the modeled resistances, the reaction rate was predominantly limited by the liquid–solid mass transfer of H_2 towards the external catalyst surface and/or the internal diffusion of H_2 combined with kinetics (i.e., when $k = k_{est}$), given the dominant contributions of $\Omega_{H_2,L-S}$ and/or $\Omega_{H_2,R}$ (Fig. 6). This does not necessarily represent the real-case scenario since $\Omega_{H_2,R}$ is very likely overestimated, primarily because of an underestimation of the overall reaction rate constant k (cf. Supplementary Material, Section S7). Since this estimation is just an order of magnitude analysis and the actual k value should be higher, the influence of $\Omega_{H_2,R}$ was also evaluated with a higher and more realistic k value for a better illustration (e.g., $k = 3k_{est}$ as shown in this figure). In the latter case, $\Omega_{H_2,R}$ becomes much less significant under our experimental conditions. For such k value the external liquid–solid transfer of H_2 is dominant under nearly all tested reaction conditions as indicated by the much higher value of $\Omega_{H_2,L-S}$ over the other resistance values. Hence, it is possible that the overall reaction rate is mainly limited by the external liquid–solid mass transfer of H_2 over most reaction conditions. This high $\Omega_{H_2,L-S}$ is mainly because of the relatively large catalyst particles (0.3 or 0.45 mm) used, resulting in a relatively low specific catalyst area (Eq. (11)) and therewith reducing the external liquid–solid mass transfer rate of H_2 (Eq. (9)).

To confirm that the actual kinetic parameter (k) is underestimated by k_{est} such that the actual $\Omega_{H_2,R}$ should be unimportant in the resistance under our experimental conditions, the above model is further simplified by considering very fast kinetics. Although faster kinetics results in a (slightly) lower effectiveness factor by the increased Thiele modulus (cf. Section S8 in the Supplementary Material), the combined rate of internal diffusion and surface reaction will increase so that $\Omega_{H_2,R}$ becomes significantly smaller (Eq. (26)). Then, the overall reaction rate is fully determined by the combined gas–liquid and external liquid–solid mass transfer. Accordingly, the H_2 consumption rate is rewritten as

$$r_{H_2} = \frac{C_{H_2,G}/H}{\frac{1}{V_{bed} k_L a_i} + \frac{1}{\alpha w_c k_S a_c}} \quad (27)$$

From Eqs. (1), (19) and (27), the modeled LA conversion is simplified as

$$X_{LA} = \frac{r_{LA}}{Q_{L,0} C_{LA,0}} = \frac{C_{H_2,G}/H}{Q_{L,0} C_{LA,0} \left(\frac{1}{V_{bed} k_L a_i} + \frac{1}{\alpha w_c k_S a_c} \right)} \quad (28)$$

The experimental LA conversion is generally described by Eq. (28) with an acceptable accuracy under all reaction conditions tested (Fig. 3). This simplified model also corresponds roughly with experiments conducted at a higher initial LA concentration of 10 wt% (cf. Supplementary Material, Section S3 for more details). Thus, the actual k value should be indeed higher than k_{est} (cf. Supplementary Material, Section S7) and the reaction under the present experiments is predominantly limited by the combined gas–liquid and liquid–solid mass transfer of H_2 from the gas–liquid interface towards the external catalyst surface (and especially by latter under the majority of conditions). For a more accurate kinetic description towards obtaining the fully informative model, dedicated kinetic studies on the hydrogenation of LA to HPA and GVL in 1,4-dioxane are required.

By comparing the resistance trends, the contribution of individual reaction parameters to each H_2 transfer or reaction step, and further on to the overall reaction rate, could be made clear over a wide range of conditions (Fig. 6). Here, the influence of the combined internal diffusion/kinetic resistance ($\Omega_{H_2,R}$) is roughly evaluated with the illustrative case of $k = 3k_{est}$ (since the exact k value is unknown).

Each resistance decreases upon increasing the mixture flow rate (with a fixed gas–liquid flow ratio and *WHSV* being kept equal by varying the bed length; Fig. 6a). This is because the bed length is proportional to the catalyst weight (or bed volume), and an increase of this negatively contributes to all resistances (Eqs. (24)–(26)). This also explains the observed LA conversion increase with the flow rate increase (Fig. 3a). It should be noted that at lower flow rates (corresponding to a shorter bed), the measured LA conversion was underestimated by the model (Fig. 3a). Under such low flow rates, it might take (much) longer time for the upstream slug flow to develop into liquid-dominated slug flow in the catalyst bed. This would lead to a lower mass transfer rate in the bed (at least near the inlet section) and thus the overall reaction performance turned out to be somewhat significantly lower than predicted by the model.

The measured LA conversion gradually increased with the increasing gas to liquid flow ratio for a given mixture flow rate as approximately predicted by the simplified model (Fig. 3b). However, the external liquid–solid mass transfer resistance of H_2 (i.e., the most dominant one) is actually (slightly) increased with the gas to liquid flow ratio (Fig. 6b). The increase in the LA conversion at higher flow ratios is thus mainly attributed to the reduced liquid flow rate ($Q_{L,0}$; cf. Eq. (28)). The gas–liquid mass transfer resistance is also slightly increased by the higher gas to liquid flow ratio (Fig. 6b), whereas the combined internal diffusion/kinetic resistance seems not (significantly) affected by this.

The H_2 pressure does not significantly affect the mass transfer coefficients ($k_L a_i$ and $k_S a_c$; Eqs. (8) and (13)), but does affect the H_2 concentration in the liquid phase. The H_2 pressure is linearly proportional to $C_{H_2,I,L}$ (Eq. (6)) and thus significantly increases X_{LA} under otherwise unchanged reaction conditions (Eq. (28); Fig. 3c). The pressure does not affect the gas–liquid and external liquid–solid mass transfer resistances (Eqs. (7) and (9)). An increase in pressure does positively affect the internal diffusion/kinetic resistance, mainly due to the half-order dependency of H_2 on the kinetic rate (Fig. 6c).

The reaction temperature, under otherwise unchanged conditions, resulted in a significantly higher LA conversion (Fig. 3d). This is mainly due to its positive effect on the gas–liquid and (external) liquid–solid mass transfer rates of H_2 (e.g., by decreasing the value of Henry coefficient (Eqs. (6) and (7)) and increasing the mass diffusivity (Eqs. (8) and (12))). For the temperature tested in this work (between 70 and 130 °C), the overall reaction rate is preliminary determined by the external liquid–solid mass transfer rate. However, at lower temperatures the intrinsic kinetic rate would become sufficiently small, and the liquid phase mass transfer coefficient ($k_L a_i$; Eq. (8)) is lowered more than the external liquid–solid mass transfer coefficient ($k_S a_c$; Eq. (12)). Thus, a temperature reduction results in a more appreciable increase in $\Omega_{H_2,G-L}$ and $\Omega_{H_2,R}$ as compared to $\Omega_{H_2,L-S}$, making the former two resistances to play a more dominant role at relatively low temperatures (Fig. 6d).

The change in the relative importance of each resistance is further seen from the modeled influence of catalyst particle size as depicted in Fig. 6e. Both the gas–liquid and external liquid–solid mass transfer resistances decrease with a reduction of the particle size, due to the improved mass transfer coefficients (Eqs. (8) and (12)) and the specific catalyst surface area. This corresponds with the measured LA conversion increase in experiments using smaller catalyst particles (d_p = 0.3 mm; Fig. 3e). Under the involved conditions, the model suggests that $\Omega_{H_2,L-S}$ is lower than $\Omega_{H_2,R}$ when d_p is below ca. 0.03 mm

(i.e., for $k = 3k_{est}$; Fig. 6e). Furthermore, for d_p below ca. 0.14 mm $\Omega_{H_2,G-L}$ exceeds $\Omega_{H_2,L-S}$ and as such should also be significantly lowered (e.g., by increasing the temperature; cf. Fig. 6d). The use of smaller catalyst particles in the current experiments may have resulted in a slightly higher pressure drop over the packed bed microreactor [59,81], so that for a given outlet pressure the average pressure over the reactor may have been even higher. This would increase the H_2 concentration in the liquid phase, which in turn attributes to a further increase in the (gas–liquid and liquid–solid) mass transfer rate of H_2 (Eqs. (7) and (9)). However, the estimated pressure drop (i.e., calculated by the empirical correlation proposed by Zhang *et al.* [59]) was too insignificant to have a noteworthy contribution.

In the model, the mass transfer resistance of LA is not considered since it has been shown above (under the benchmarking conditions) that the liquid–solid mass transfer coefficient of LA and its initial concentration are much higher than those of H_2, and the internal diffusion of LA within the catalyst pores is faster than that of H_2 (i.e., $\eta_{LA} > \eta_{H_2}$) under most reaction conditions. Only when the bulk LA in the liquid is almost depleted (i.e., at a close to full conversion occurred near the end of the packed bed), the external and internal liquid–solid mass transfer resistances of LA start to have a more significant influence on the reaction rate. However, throughout the entire packed bed this influence on the overall reaction rate is expected negligible.

A first attempt to apply this model in alternative packed bed configurations (i.e., by the immersion of inert SiC particles in the catalyst bed) has been made for the same reaction (cf. Section S9 in the Supplementary Material). The measured microreactor performance appeared much lower than the prediction of the simplified model (i.e., even when considering the lower catalyst weight used), which is probably caused by an incomplete catalyst wetting by 1,4-dioxane as a result of the dilution of catalyst bed with SiC. Other packed bed microreactor characteristics (e.g., particle shape, microreactor inner diameter and geometry) need to be tested for a further validation of this model, which is part of our ongoing work.

In the current model, the reaction is simply considered as 0.5th order in H_2 and zero order in LA. This reaction order dependency is in line with literature observations on the Ru/C-catalyzed hydrogenation of LA (in water) [26,27] as well as hydrogenation of other liquid substrates (e.g., glucose to sorbitol [32], cyclohexene to cyclohexane [78]). The overall reaction rate constant (k) was roughly estimated from the data of Ftouni *et al.* [24], which seems to also suggest that the reaction order might have changed to 1st order at high LA conversions (i.e., when the GVL selectivity is assumed 100% and the LA concentration is typically low). Although this has to be further checked in future dedicated kinetic studies, k values were also approximately estimated for the hypothetical case of a (0.5, 1)-th order reaction in LA hydrogenation (note that also in this case the actual k value should be higher; cf. Section S7 in the Supplementary Material). Under such circumstances, the current model (Eq. (20)) can be further extended to estimate the LA conversion (cf. Section S10 in the Supplementary Material). Given the additional facts that the initial LA concentration used in this study is relatively high (5–10 wt%), the measured LA conversion in microreactors is mostly below ca. 80% and generally in a good agreement with the current model prediction, the assumption of a (0.5, 0)-th order reaction is expected very reasonable.

4. Microreactor optimization strategy

A relatively low selectivity towards GVL was obtained (i.e., in the case that LA was not fully converted yet; Fig. 3) in our experiments. This is mainly because the transformation of the HPA intermediate towards GVL was slower than the formation of HPA from LA under the conditions tested. The formation of GVL from HPA is accelerated by the acidity of the liquid phase and as such adding small amounts of sulfuric acid can significantly improve the GVL yield in the Ru/C catalyzed hydrogenation of LA in 1,4-dioxane [25]. Despite this, the LA consumption rate was highly limited by the external liquid–solid mass transfer of H_2. Given the acceptable accuracy of the developed microreactor model under mass transfer limited conditions (i.e., Eq. (28), or Eq. (20) provided that the accurate kinetic parameters are available), this allows to predict favorable design parameters for further reaction optimization. To increase the LA consumption rate (and therewith the GVL production rate) per catalyst weight, external liquid–solid mass transfer limitations should be overcome. This can be done by increasing the flow velocity (i.e., the bed length should be increased as well to remain the same *WHSV*), as inferred from Eq. (13). Furthermore, temperature and H_2 pressure accelerate both the reaction kinetics and physical mass transfer rates. Especially because of the relatively low solubility of H_2 in 1,4-dioxane [73], elevated H_2 pressures are essential to promote the (external liquid–solid) H_2 mass transfer [48]. In the current setup much higher temperatures and pressures were not attainable, due to the limited resistance of the PFA capillary and PEEK connectors used. Alternative (capillary) microreactor/connector materials (e.g., stainless steel) may benefit the reaction performance from operation under elevated conditions, although the use of such non-transparent materials makes the packed bed filling procedure and the analysis of gas–liquid hydrodynamics more difficult. Furthermore, the influence of liquid to solid particle wettability on the liquid–solid mass transfer characteristics should be studied in packed bed microreactors (e.g., in the case of bed dilution) to prevent wall-channeling and improve the reaction performance (cf. Section S9 in the Supplementary Material).

The reaction rate may also be enhanced under relatively mild reaction conditions. For instance, the use of smaller diameter catalyst particles significantly increases the specific catalytic surface area and accelerates the (external) liquid–solid mass transfer (Eqs. (13) and (25)). However, a downside is the higher pressure drop possibly generated over the microchannel [59,81]. Thus, a compromise between the maximum allowable pressure drop in the microreactor and the acceptable performance improvement needs to be considered. In this regard, the immersion of very fine solid catalyst powders in a packed bed configuration may become less appealing for practical applications. Alternative methods for the incorporation of solid catalysts in microreactors with a high specific catalyst area, but without excessive pressure drop penalty, are by wall-coating or the use of hollow spheres or catalytic foams [82,83]. In such foams, relatively high mass transfer performance could be obtained [84]. However, the development of these may require cumbersome catalyst incorporation and/or production techniques [38]. Another less reported method is to disperse the catalyst as nano- or microparticles in a continuous liquid flow (i.e., forming a gas–liquid slurry). In such configuration, relatively small catalyst particles can be used while still benefitting from the enhanced heat and (gas–liquid) mass transfer in microreactors, at the possible cost of channel fouling or local blockage leading to the device malfunction [85].

5. Conclusions

The Ru/C catalyzed hydrogenation of LA to GVL was performed in packed bed microreactors made of PFA with H_2 gas as the hydrogen donor and 1,4-dioxane as the solvent. The influence of operating conditions (i.e., flow rate, gas to liquid flow ratio, temperature, pressure and catalyst particle size) on the reaction performance was investigated. HPA was identified as an abundantly formed intermediate, which was only further converted to GVL once the majority of LA was consumed. At 130 °C and 12 bar H_2, an LA conversion of 100% and a GVL yield of 84% were obtained at a weight hourly space velocity of the liquid phase (*WHSV*) of 3.0 $g_{feed}/(g_{cat} \cdot h)$. A microreactor model was developed by considering the respective rates of gas–liquid and external liquid–solid mass transfer, internal diffusion combined with surface reaction based on the literature correlations and data. The model was able to describe the LA conversion as a function of the different reaction

conditions, provided that the internal diffusion and kinetic rates were not considered rate limiting. Under the majority of operating conditions (70–130 °C and 9–15 bar), the reaction was found limited by external liquid–solid mass transfer of H_2, primarily due to the relatively low flow rates used and relatively large catalyst particles (diameter of 0.3 or 0.45 mm) in the bed. The developed model allows to propose a further optimization strategy for reaction improvement of the Ru/C catalyzed hydrogenation of LA to GVL in packed bed microreactors.

The modeling approach of this work may guide industrial applications (e.g., numbered-up packed bed microreactors for hydrogenations in fine chemical/pharmaceutical synthesis), under the preconditions that gas–liquid–solid hydrodynamics and mass transfer characteristics (i.e., k_La_i and k_S) as well as reaction kinetics are well described. Gas–liquid hydrogenation reactions are often limited by external or internal liquid–solid mass transfer limitations. Under such circumstances, (the often expensive) heterogeneous catalyst is not optimally utilized. With the aid of such modelling, operating conditions where mass transfer limitations are avoided may be identified for an optimal catalyst usage (e.g., in the kinetic regime).

Declaration of Competing Interest

The authors declare that they have no known competing financial interests or personal relationships that could have appeared to influence the work reported in this paper.

Acknowledgements

This work was financially supported by the University of Groningen (startup package in the area of green chemistry and technology for Jun Yue).

Appendix A. Supplementary data

Supplementary data to this article can be found online at https://doi.org/10.1016/j.cej.2020.125750.

References

[1] J.N. Chheda, G.W. Huber, J.A. Dumesic, Liquid-phase catalytic processing of biomass-derived oxygenated hydrocarbons to fuels and chemicals, Angew. Chem. Int. Ed. 46 (2007) 7164–7183, https://doi.org/10.1002/anie.200604274.
[2] T. Werpy, G. Petersen, Top Value Added Chemicals From Biomass: volume I. Results of Screening For Potential Candidates from Sugars and Synthesis Gas, National Renewable Energy Lab., Golden, CO (US), 2004 doi:10.2172/926125.
[3] A. Corma, S. Iborra, A. Velty, Chemical routes for the transformation of biomass into chemicals, Chem. Rev. 107 (2007) 2411–2502, https://doi.org/10.1021/cr050989d.
[4] K. Yan, C. Jarvis, J. Gu, Y. Yan, Production and catalytic transformation of levulinic acid: A platform for speciality chemicals and fuels, Renew. Sustain. Energy Rev. 51 (2015) 986–997, https://doi.org/10.1016/j.rser.2015.07.021.
[5] I.T. Horváth, H. Mehdi, V. Fábos, L. Boda, L.T. Mika, γ-Valerolactone-a sustainable liquid for energy and carbon-based chemicals, Green Chem. 10 (2008) 238–242, https://doi.org/10.1039/b712863k.
[6] D.M. Alonso, S.G. Wettstein, J.A. Dumesic, Gamma-valerolactone, a sustainable platform molecule derived from lignocellulosic biomass, Green Chem. 15 (2013) 584–595, https://doi.org/10.1039/c3gc37065h.
[7] K. Yan, Y. Yang, J. Chai, Y. Lu, Catalytic reactions of gamma-valerolactone: A platform to fuels and value-added chemicals, Appl. Catal. B Environ. 179 (2015) 292–304, https://doi.org/10.1016/j.apcatb.2015.04.030.
[8] Y. Gu, F. Jérôme, Bio-based solvents: An emerging generation of fluids for the design of eco-efficient processes in catalysis and organic chemistry, Chem. Soc. Rev. 42 (2013) 9550–9570, https://doi.org/10.1039/c3cs60241a.
[9] S.G. Wettstein, D.M. Alonso, Y. Chong, J.A. Dumesic, Production of levulinic acid and gamma-valerolactone (GVL) from cellulose using GVL as a solvent in biphasic systems, Energy Environ. Sci. 5 (2012) 8199–8203, https://doi.org/10.1039/c2ee22111j.
[10] J.M.R. Gallo, D.M. Alonso, M.A. Mellmer, J.A. Dumesic, Production and upgrading of 5-hydroxymethylfurfural using heterogeneous catalysts and biomass-derived solvents, Green Chem. 15 (2013) 85–90, https://doi.org/10.1039/c2gc36536g.
[11] A. Kumar, Y.E. Jad, J.M. Collins, F. Albericio, B.G. de la Torre, Microwave-assisted green solid-phase peptide synthesis using γ-valerolactone (GVL) as solvent, ACS Sustain. Chem. Eng. 6 (2018) 8034–8039, https://doi.org/10.1021/acssuschemeng.8b01531.
[12] D. Fegyverneki, L. Orha, G. Láng, I.T. Horváth, Gamma-valerolactone-based solvents, Tetrahedron 66 (2010) 1078–1081, https://doi.org/10.1016/j.tet.2009.11.013.
[13] L.E. Manzer, Catalytic synthesis of α-methylene-γ-valerolactone: A biomass-derived acrylic monomer, Appl. Catal. A Gen. 272 (2004) 249–256, https://doi.org/10.1016/j.apcata.2004.05.048.
[14] L. Deng, Y. Zhao, J. Li, Y. Fu, B. Liao, Q.X. Guo, Conversion of levulinic acid and formic acid into γ-valerolactone over heterogeneous catalysts, ChemSusChem 3 (2010) 1172–1175, https://doi.org/10.1002/cssc.201000163.
[15] A.M.R. Galletti, C. Antonetti, V. de Luise, M. Martinelli, A sustainable process for the production of γ-valerolactone by hydrogenation of biomass-derived levulinic acid, Green Chem. 14 (2012) 688–694, https://doi.org/10.1039/c2gc15872h.
[16] M. Chia, J.A. Dumesic, Liquid-phase catalytic transfer hydrogenation and cyclization of levulinic acid and its esters to γ-valerolactone over metal oxide catalysts, Chem. Commun. 47 (2011) 12233–12235, https://doi.org/10.1039/c1cc14748j.
[17] W.R.H. Wright, R. Palkovits, Development of heterogeneous catalysts for the conversion of levulinic acid to γ-valerolactone, ChemSusChem 5 (2012) 1657–1667, https://doi.org/10.1002/cssc.201200111.
[18] S. Dutta, I.K.M. Yu, D.C.W. Tsang, Y.H. Ng, Y.S. Ok, J. Sherwood, J.H. Clark, Green synthesis of gamma-valerolactone (GVL) through hydrogenation of biomass-derived levulinic acid using non-noble metal catalysts: A critical review, Chem. Eng. J. 372 (2019) 992–1006, https://doi.org/10.1016/j.cej.2019.04.199.
[19] P.P. Upare, J.M. Lee, D.W. Hwang, S.B. Halligudi, Y.K. Hwang, J.S. Chang, Selective hydrogenation of levulinic acid to γ-valerolactone over carbon-supported noble metal catalysts, J. Ind. Eng. Chem. 17 (2011) 287–292, https://doi.org/10.1016/j.jiec.2011.02.025.
[20] Z.P. Yan, L. Lin, S. Liu, Synthesis of γ-valerolactone by hydrogenation of biomass-derived levulinic acid over Ru/C catalyst, Energy Fuels 23 (2009) 3853–3858, https://doi.org/10.1021/ef900259h.
[21] P.P. Upare, M. Lee, S.K. Lee, J.W. Yoon, J. Bae, D.W. Hwang, U.H. Lee, J.S. Chang, Y.K. Hwang, Ru nanoparticles supported graphene oxide catalyst for hydrogenation of bio-based levulinic acid to cyclic ethers, Catal. Today 265 (2016) 174–183, https://doi.org/10.1016/j.cattod.2015.09.042.
[22] A.S. Piskun, J.E. de Haan, E. Wilbers, H.H. van de Bovenkamp, Z. Tang, H.J. Heeres, Hydrogenation of levulinic acid to γ-valerolactone in water using millimeter sized supported Ru catalysts in a packed bed reactor, ACS Sustain. Chem. Eng. 4 (2016) 2939–2950, https://doi.org/10.1021/acssuschemeng.5b00774.
[23] W. Luo, U. Deka, A.M. Beale, E.R.H. van Eck, P.C.A. Bruijnincx, B.M. Weckhuysen, Ruthenium-catalyzed hydrogenation of levulinic acid: Influence of the support and solvent on catalyst selectivity and stability, J. Catal. 301 (2013) 175–186, https://doi.org/10.1016/j.jcat.2013.02.003.
[24] J. Ftouni, A. Muñoz-Murillo, A. Goryachev, J.P. Hofmann, E.J.M. Hensen, L. Lu, C.J. Kiely, P.C.A. Bruijnincx, B.M. Weckhuysen, ZrO_2 is preferred over TiO_2 as support for the Ru-catalyzed hydrogenation of levulinic acid to γ-valerolactone, ACS Catal. 6 (2016) 5462–5472, https://doi.org/10.1021/acscatal.6b00730.
[25] J. Ftouni, H.C. Genuino, A. Muñoz-Murillo, P.C.A. Bruijnincx, B.M. Weckhuysen, Influence of sulfuric acid on the performance of ruthenium-based catalysts in the liquid-phase hydrogenation of levulinic acid to γ-valerolactone, ChemSusChem 10 (2017) 2891–2896, https://doi.org/10.1002/cssc.201700768.
[26] O.A. Abdelrahman, A. Heyden, J.Q. Bond, Analysis of kinetics and reaction pathways in the aqueous-phase hydrogenation of levulinic acid to form γ-valerolactone over Ru/C, ACS Catal. 4 (2014) 1171–1181, https://doi.org/10.1021/cs401177p.
[27] A.S. Piskun, H.H. van de Bovenkamp, C.B. Rasrendra, J.G.M. Winkelman, H.J. Heeres, Kinetic modeling of levulinic acid hydrogenation to γ-valerolactone in water using a carbon supported Ru catalyst, Appl. Catal. A Gen. 525 (2016) 158–167, https://doi.org/10.1016/j.apcata.2016.06.033.
[28] S. Galvagno, G. Capannelli, G. Neri, A. Donato, R. Pietropaolo, Hydrogenation of cinnamaldehyde over Ru/C catalysts: effect of Ru particle size, J. Mol. Catal. 64 (1991) 237–246, https://doi.org/10.1016/0304-5102(91)85115-I.
[29] V.A. Sifontes Herrera, O. Oladele, K. Kordás, K. Eränen, J.P. Mikkola, D.Y. Murzin, T. Salmi, Sugar hydrogenation over a Ru/C catalyst, J. Chem. Technol. Biotechnol. 86 (2011) 658–668, https://doi.org/10.1002/jctb.2565.
[30] P. Panagiotopoulou, N. Martin, D.G. Vlachos, Liquid-phase catalytic transfer hydrogenation of furfural over homogeneous Lewis acid-Ru/C catalysts, ChemSusChem 8 (2015) 2046–2054, https://doi.org/10.1002/cssc.201500212.
[31] L. Negahdar, M.G. Al-Shaal, F.J. Holzhäuser, R. Palkovits, Kinetic analysis of the catalytic hydrogenation of alkyl levulinates to γ-valerolactone, Chem. Eng. Sci. 158 (2017) 545–551, https://doi.org/10.1016/j.ces.2016.11.007.
[32] E. Crezee, B.W. Hoffer, R.J. Berger, M. Makkee, F. Kapteijn, J.A. Moulijn, Three-phase hydrogenation of D-glucose over a carbon supported ruthenium catalyst - Mass transfer and kinetics, Appl. Catal. A Gen. 251 (2003) 1–17, https://doi.org/10.1016/S0926-860X(03)00587-8.
[33] D.G. Blackmond, A. Armstrong, V. Coombe, A. Wells, Water in organocatalytic processes: Debunking the myths, Angew. Chem. Int. Ed. 46 (2007) 3798–3800, https://doi.org/10.1002/anie.200604952.
[34] J. Molleti, M.S. Tiwari, G.D. Yadav, Novel synthesis of Ru/OMS catalyst by solvent-free method: Selective hydrogenation of levulinic acid to γ-valerolactone in aqueous medium and kinetic modelling, Chem. Eng. J. 334 (2018) 2488–2499, https://doi.org/10.1016/j.cej.2017.11.125.
[35] P.B. Weisz, C.D. Prater, Interpretation of measurements in experimental catalysis, Adv. Catal. 6 (1954) 143–196, https://doi.org/10.1016/S0360-0564(08)60390-9.
[36] M. Irfan, T.N. Glasnov, C.O. Kappe, Heterogeneous catalytic hydrogenation reactions in continuous-flow reactors, ChemSusChem 4 (2011) 300–316, https://doi.org/10.1002/cssc.201000354.
[37] K.F. Jensen, Flow chemistry – Microreaction technology comes of age, AIChE J. 63

(2017) 858–869, https://doi.org/10.1002/aic.15642.
[38] V. Hessel, P. Angeli, A. Gavriilidis, H. Löwe, Gas-liquid and gas-liquid-solid microstructured reactors: Contacting principles and applications, Ind. Eng. Chem. Res. 44 (2005) 9750–9769, https://doi.org/10.1021/ie0503139.
[39] M.N. Kashid, A. Renken, L. Kiwi-Minsker, Gas-liquid and liquid-liquid mass transfer in microstructured reactors, Chem. Eng. Sci. 66 (2011) 3876–3897, https://doi.org/10.1016/j.ces.2011.05.015.
[40] M.N. Kashid, L. Kiwi-Minsker, Microstructured reactors for multiphase reactions: State of the art, Ind. Eng. Chem. Res. 48 (2009) 6465–6485, https://doi.org/10.1021/ie8017912.
[41] J. Fischer, C. Liebner, H. Hieronymus, E. Klemm, Maximum safe diameters of microcapillaries for a stoichiometric ethene/oxygen mixture, Chem. Eng. Sci. 64 (2009) 2951–2956, https://doi.org/10.1016/j.ces.2009.03.038.
[42] C.G. Frost, L. Mutton, Heterogeneous catalytic synthesis using microreactor technology, Green Chem. 12 (2010) 1687–1703, https://doi.org/10.1039/c0gc00133c.
[43] A. Tanimu, S. Jaenicke, K. Alhooshani, Heterogeneous catalysis in continuous flow microreactors: A review of methods and applications, Chem. Eng. J. 327 (2017) 792–821, https://doi.org/10.1016/j.cej.2017.06.161.
[44] J. Yue, Multiphase flow processing in microreactors combined with heterogeneous catalysis for efficient and sustainable chemical synthesis, Catal. Today 308 (2018) 3–19, https://doi.org/10.1016/j.cattod.2017.09.041.
[45] K. Tadele, S. Verma, M.A. Gonzalez, R.S. Varma, A sustainable approach to empower the bio-based future: Upgrading of biomass via process intensification, Green Chem. 19 (2017) 1624–1627, https://doi.org/10.1039/c6gc03568j.
[46] S. Kressirer, L.N. Protasova, M.H.J.M. de Croon, V. Hessel, D. Kralisch, Removal and renewal of catalytic coatings from lab- and pilot-scale microreactors, accompanied by life cycle assessment and cost analysis, Green Chem. 14 (2012) 3034–3046, https://doi.org/10.1039/c2gc35803d.
[47] L. He, Y. Fan, L. Luo, J. Bellettre, J. Yue, Preparation of Pt/γ-Al_2O_3 catalyst coating in microreactors for catalytic methane combustion, Chem. Eng. J. 380 (2020) 122424, , https://doi.org/10.1016/j.cej.2019.122424.
[48] F. Trachsel, C. Hutter, P. Rudolf von Rohr, Transparent silicon/glass microreactor for high-pressure and high-temperature reactions, Chem. Eng. J. 135 (2008) 309–316, https://doi.org/10.1016/j.cej.2007.07.049.
[49] A. Faridkhou, J.N. Tourvieille, F. Larachi, Reactions, hydrodynamics and mass transfer in micro-packed beds - Overview and new mass transfer data, Chem. Eng. Process. Process Intensif. 110 (2016) 80–96, https://doi.org/10.1016/j.cep.2016.09.016.
[50] M.W. Losey, M.A. Schmidt, K.F. Jensen, Microfabricated multiphase packed-bed reactors: Characterization of mass transfer and reactions, Ind. Eng. Chem. Res. 40 (2001) 2555–2562, https://doi.org/10.1021/ie000523f.
[51] A. Attou, G. Ferschneider, A two-fluid hydrodynamic model for the transition between trickle and pulse flow in a cocurrent gas-liquid packed-bed reactor, Chem. Eng. Sci. 55 (2000) 491–511, https://doi.org/10.1016/S0009-2509(99)00344-9.
[52] N. Márquez, P. Castaño, M. Makkee, J.A. Moulijn, M.T. Kreutzer, Dispersion and holdup in multiphase packed bed microreactors, Chem. Eng. Technol. 31 (2008) 1130–1139, https://doi.org/10.1002/ceat.200800198.
[53] N. Márquez, P. Castaño, J.A. Moulijn, M. Makkee, M.T. Kreutzer, Transient behavior and stability in miniaturized multiphase packed bed reactors, Ind. Eng. Chem. Res. 49 (2010) 1033–1040, https://doi.org/10.1021/ie900694r.
[54] J.A. Moulijn, M. Makkee, R.J. Berger, Catalyst testing in multiphase micro-packed-bed reactors; criterion for radial mass transport, Catal. Today 259 (2016) 354–359, https://doi.org/10.1016/j.cattod.2015.05.025.
[55] A. Faridkhou, F. Larachi, Hydrodynamics of gas-liquid cocurrent flows in micro-packed beds-wall visualization study, Ind. Eng. Chem. Res. 51 (2012) 16495–16504, https://doi.org/10.1021/ie301709x.
[56] A. Faridkhou, F. Larachi, Two-phase flow hydrodynamic study in micro-packed beds - Effect of bed geometry and particle size, Chem. Eng. Process. Process Intensif. 78 (2014) 27–36, https://doi.org/10.1016/j.cep.2014.02.005.
[57] A. Faridkhou, M. Hamidipour, F. Larachi, Hydrodynamics of gas-liquid micro-fixed beds – Measurement approaches and technical challenges, Chem. Eng. J. 223 (2013) 425–435, https://doi.org/10.1016/j.cej.2013.03.014.
[58] N. Al-Rifai, F. Galvanin, M. Morad, E. Cao, S. Cattaneo, M. Sankar, V. Dua, G. Hutchings, A. Gavriilidis, Hydrodynamic effects on three phase micro-packed bed reactor performance – Gold-palladium catalysed benzyl alcohol oxidation, Chem. Eng. Sci. 149 (2016) 129–142, https://doi.org/10.1016/j.ces.2016.03.018.
[59] J. Zhang, A.R. Teixeira, L.T. Kogl, L. Yang, K.F. Jensen, Hydrodynamics of gas-liquid in micropacked beds: Pressure drop, liquid holdup, and two-phase model, AIChE J. 63 (2017) 4694–4704, https://doi.org/10.1002/aic.15807.
[60] T. Inoue, M.A. Schmidt, K.F. Jensen, Microfabricated multiphase reactors for the direct synthesis of hydrogen peroxide from hydrogen and oxygen, Ind. Eng. Chem. Res. 46 (2007) 1153–1160, https://doi.org/10.1021/ie061277w.
[61] S. Tadepalli, R. Halder, A. Lawal, Catalytic hydrogenation of o-nitroanisole in a microreactor: Reactor performance and kinetic studies, Chem. Eng. Sci. 62 (2007) 2663–2678, https://doi.org/10.1016/j.ces.2006.12.058.
[62] D. van Herk, P. Castaño, M. Makkee, J.A. Moulijn, M.T. Kreutzer, Catalyst testing in a multiple-parallel, gas-liquid, powder-packed bed microreactor, Appl. Catal. A Gen. 365 (2009) 199–206, https://doi.org/10.1016/j.apcata.2009.06.010.
[63] X. Liu, B. Ünal, K.F. Jensen, Heterogeneous catalysis with continuous flow microreactors, Catal. Sci. Technol. 2 (2012) 2134–2138, https://doi.org/10.1039/c2cy20260c.
[64] S. Tadepalli, D. Qian, A. Lawal, Comparison of performance of microreactor and semi-batch reactor for catalytic hydrogenation of o-nitroanisole, Catal. Today 125 (2007) 64–73, https://doi.org/10.1016/j.cattod.2007.01.076.
[65] N. Cherkasov, P. Denissenko, S. Deshmukh, E.V. Rebrov, Gas-liquid hydrogenation in continuous flow – The effect of mass transfer and residence time in powder packed-bed and catalyst-coated reactors, Chem. Eng. J. 379 (2020) 122292, , https://doi.org/10.1016/j.cej.2019.122292.
[66] A. Hommes, H.J. Heeres, J. Yue, Catalytic transformation of biomass derivatives to value-added chemicals and fuels in continuous flow microreactors, ChemCatChem 11 (2019) 4671–4708, https://doi.org/10.1002/cctc.201900807.
[67] J.P. Barranco, C.G. Selma, Gas/liquid separator comprising a capacitive level sensor, U.S. Patent No. 7,895,891. 1 March, 2011.
[68] M.G. Al-Shaal, A. Dzierbinski, R. Palkovits, Solvent-free γ-valerolactone hydrogenation to 2-methyltetrahydrofuran catalysed by Ru/C: A reaction network analysis, Green Chem. 16 (2014) 1358–1364, https://doi.org/10.1039/c3gc41803k.
[69] J. Zhang, A.R. Teixeira, K.F. Jensen, Automated measurements of gas-liquid mass transfer in micropacked bed reactors, AIChE J. 64 (2018) 564–570, https://doi.org/10.1002/aic.15941.
[70] R. Langsch, J. Zalucky, S. Haase, R. Lange, Investigation of a packed bed in a mini channel with a low channel-to-particle diameter ratio: Flow regimes and mass transfer in gas-liquid operation, Chem. Eng. Process. Process Intensif. 75 (2014) 8–18, https://doi.org/10.1016/j.cep.2013.10.004.
[71] B. Tidona, S. Desportes, M. Altheimer, K. Ninck, P. Rudolf von Rohr, Liquid-to-particle mass transfer in a micro packed bed reactor, Int. J. Heat Mass Transf. 55 (2012) 522–530, https://doi.org/10.1016/j.ijheatmasstransfer.2011.11.012.
[72] C.C. Templis, N.G. Papayannakos, Liquid-to-particle mass transfer in a structured-bed minireactor, Chem. Eng. Technol. 40 (2017) 385–394, https://doi.org/10.1002/ceat.201500733.
[73] E. Brunner, Solubility of hydrogen in 10 organic solvents at 298.15, 323.15, and 373.15 K, J. Chem. Eng. Data. 30 (1985) 269–273, https://doi.org/10.1021/je00041a010.
[74] R. Sander, Compilation of Henry's law constants (version 4.0) for water as solvent, Atmos. Chem. Phys. 15 (2015) 4399–4981, https://doi.org/10.5194/acp-15-4399-2015.
[75] C.R. Wilke, P. Chang, Correlation of diffusion coefficients in dilute solutions, AIChE J. 1 (1955) 264–270, https://doi.org/10.1002/aic.690010222.
[76] N. Wakao, T. Funazkri, Effect of fluid dispersion coefficients on particle-to-fluid mass transfer coefficients in packed beds: Correlation of Sherwood numbers, Chem. Eng. Sci. 33 (1978) 1375–1384 doi:0009-2509/78/1001-1375/S02.00/0.
[77] N.K. Sinha, M. Neurock, A first principles analysis of the hydrogenation of C1–C4 aldehydes and ketones over Ru(0 0 0 1), J. Catal. 295 (2012) 31–44, https://doi.org/10.1016/j.jcat.2012.07.018.
[78] E.E. Gonzo, M. Boudart, Catalytic hydrogenation of cyclohexene: 3. Gas-phase and liquid-phase reaction on supported palladium, J. Catal. 52 (1978) 462–471, https://doi.org/10.1016/0021-9517(78)90352-4.
[79] H.S. Fogler, Diffusion and reaction, in: Elem. Chem. React. Eng., 4th ed., Pearson Education International, 2006: pp. 813–866.
[80] I. Stamatiou, F.L. Muller, Determination of mass transfer resistances in trickle bed reactors, Chem. Eng. J. 377 (2019) 119808, , https://doi.org/10.1016/j.cej.2018.08.194.
[81] S. Hofmann, A. Bufe, G. Brenner, T. Turek, Pressure drop study on packings of differently shaped particles in milli-structured channels, Chem. Eng. Sci. 155 (2016) 376–385, https://doi.org/10.1016/j.ces.2016.08.011.
[82] S.W. Kim, M. Kim, W.Y. Lee, T. Hyeon, Fabrication of hollow palladium spheres and their successful application to the recyclable heterogeneous catalyst for suzuki coupling reactions, J. Am. Chem. Soc. 124 (2002) 7642–7643, https://doi.org/10.1021/ja026032z.
[83] M.V. Twigg, J.T. Richardson, Theory and applications of ceramic foam catalysts, Chem. Eng. Res. Des. 80 (2002) 183–189, https://doi.org/10.1016/S0263-8762(02)72166-7.
[84] J.N. Tourvieille, R. Philippe, C. de Bellefon, Milli-channel with metal foams under an applied gas-liquid periodic flow: External mass transfer performance and pressure drop, Chem. Eng. J. 267 (2015) 332–346, https://doi.org/10.1016/j.cej.2014.11.084.
[85] A.K. Liedtke, F. Scheiff, F. Bornette, R. Philippe, D.W. Agar, C. de Bellefon, Liquid-solid mass transfer for microchannel suspension catalysis in gas-liquid and liquid-liquid segmented flow, Ind. Eng. Chem. Res. 54 (2015) 4699–4708, https://doi.org/10.1021/ie504523y.